NUMERICAL MODELING OF ACCRETION FLOW AROUND BLACK HOLE: STUDY OF STATISTICS AND ENERGETICS OF PLASMOIDS

M.Sc. Thesis

By:
Sirsha Nandy

DEPARTMENT OF ASTRONOMY, ASTROPHYSICS AND SPACE ENGINEERING

INDIAN INSTITUTE OF TECHNOLOGY INDORE

May, 2022

NUMERICAL MODELING OF ACCRETION FLOW AROUND BLACK HOLE: STUDY OF STATISTICS AND ENERGETICS OF PLASMOIDS

A THESIS

Submitted in partial fulfillment of the
requirements for the award of the degree
of
Master of Science

by
Sirsha Nandy

DEPARTMENT OF ASTRONOMY , ASTROPHYSICS AND SPACE ENGINEERING

INDIAN INSTITUTE OF TECHNOLOGY INDORE

May, 2022

INDIAN INSTITUTE OF TECHNOLOGY INDORE

CANDIDATE'S DECLARATION

I hereby certify that the work which is being presented in the thesis entitled **Numerical Modeling of Accretion Flow around Black Hole: Study of Statistics and Energetics of Plasmoids** in the partial fulfillment of the requirements for the award of the degree of **MASTER OF SCIENCE** and submitted in the **Department of Astronomy, Astrophysics and Space Engineering (DAASE), Indian Institute of Technology Indore**, is an authentic record of my own work carried out during the time period from July, 2021 to May, 2022 under the supervision of Dr. Bhargav Vaidya, Assistant Professor, DAASE, IIT Indore.

The matter presented in this thesis has not been submitted by me for the award of any other degree of this or any other institute.

Sirsha Nandy.

23/05/2022

Sirsha Nandy

This is to certify that the above statement made by the candidate is correct to the best of my/our knowledge.

23-05-2022

Signature of the Supervisor of

M.Sc. (with date)

Dr. Bhargav Vaidya

Sirsha Nandy has successfully given his M.Sc. Oral Examination held on **05 May 2022**.

Manoneeta Chakraborty	23-05-2022	24/5/22
Signature of PSPC Member #1 Date: 23/05/2022	Signature of PSPC Member #2 Date:	Signature of PSPC Member #3 Date:
		S. Das
Signature(s) of Supervisor(s). Date: 23-05-2022	Signature of M.Sc. Co-Ordinator Date: 25-05-2022	Convener, DPGC Date: 26/05/2022

Manoneeta Chakraborty

Signature of HoD (Officiating)
Date: 26/05/2022

Acknowledgements

I am indebted to my supervisor, Dr. Bhargav Vaidya for his continual encouragement and guidance through the phases of this one-year long research project. He has been extremely supportive and helpful throughout the entire course of this project. I can safely say that he is the primary source of inspiration and motivation that I am so passionate about MHD simulation at this stage and want to pursue further research on the same topic. He has always encouraged me to fight against anxiety and nervousness and boosted my confidence at critical times. Besides technical lessons, he has also imparted lessons to mould my personality and develop my character to be a successful professional researcher in future.

I also want to thank my PSPC members Dr. Manoneeta Chakraborty, Dr. Amit Shukla and Dr. Debajyoti Sarkar for their kind suggestions and advices to improve upon certain aspects of my thesis. Discussions with them and other faculty members of our department have always been insightful and enlightening for me that broadened my research perspective and scientific vision.

Thanks to a couple of extensive discussions with Dr. Indu Kalpa Dihingia, who was a postdoc in our lab during the first stage of my project, I was able to discover the first motivation and passion to begin working on this topic, which was somewhat new to me at the time. He was quite instrumental in motivating and energizing me at times when I really felt bored and demotivated. I learnt a great deal of technical stuffs from him regarding my project work in GRMHD. He always iterated the importance of literature survey to eventually build a habit of the same in me which, I believe, will be of great help in my future career. Along with these, he always used to bring vitality and liveliness with his presence, witty remarks and exceptional culinary skills, of course.

I also want to thank my senior PhD students for their important advices and suggestions regarding both academic and non-academic activities through the entire duration of my post-graduate course in IITI. I have spent plenty of quality time enjoying the company of my batchmates, seniors and juniors that was thoroughly rejuvenating and refreshing.

Also, I want to convey my sincere gratitude to my family members for thoroughly supporting me both morally and financially from the very beginning of this journey. Finally, I want to thank our department, DAASE for giving me the opportunity to carry out my project in a really comfortable and work-friendly environment.

Abstract

Flares from close proximity of black hole neighborhood (in AGN and BH-XRBs) and the orbital motion of a luminous blob around the galactic center have recently been observed, indicating rich and complex magnetohydrodynamics in the core accretion zone (tens of gravitational radii). Light curves of such sources with rapid variability appear to have a time scale that is substantially shorter than the event horizon's light-crossing time scale. As a result of the causality condition, this time scale corresponds to a few Schwarzschild radii of the emitting region's length scales. The observations from such regions can be consistently explained by the non-thermal radiation from the plasmoids both in terms of time scale and energetics. Plasmoids are blobs of plasma carrying highly energetic particles formed in the magnetic reconnection process. In the finite physical resistivity regime, the magnetic reconnection process is an efficient method for converting magnetic energy into thermal dissipation and kinetic energy of the particles in the accreting fluid. In order to investigate the dynamics and evolution of such system, In the framework of General Relativistic Magnetohydrodynamics (GRMHD), a resistive axisymmetric geometrically thin accretion disc in hydrodynamic equilibrium is numerically set up around a maximally spinning Kerr black hole. Numerical simulations in GRMHD framework are performed with the thin resistive disk up to a time of $t = 2000GM/c^3$, taking two distinct ohmic resistivity values, moderate and low. For the mildly resistive disk, we investigate the size distribution and energetics of the resultant plasmoids that are formed in the black hole magnetosphere region. The generation and size distribution of plasmoids, for which the substantial kinetic energy released in reconnection events in the region with high magnetization outweighs the gravitational potential energy of the black hole, are examined. For detecting outgoing plasmoids, we employ the Bernoulli parameter distribution. The plasmoids are located in the 2D simulation snapshot using technique of binary opening as opposed to the conventional technique of detecting X-points and O-points. A different study on the size distribution of plasmoids formed via explosive magnetic reconnection in a simple system of double current sheet is also carried out in resistive MHD framework to validate the detection technique. We obtain reasonable results from the study which are physically significant. We also address the plasmoids' energy outputs quantitatively, which could account for later flaring activity in AGNs. We use a very simple model to do so, assuming that a fraction of the ohmic heat energy contributes to non-thermal plasmoid emission. A number of free parameters associated with the energy relation are explored against range of different values to obtain the optimum ones. Finally, we show the non-thermal energy output, converted into suitable physical units, does in fact matches with observation of energy output of AGN flares.

Contents

List of Figures

Chapter 1

Introduction

Active Galactic Nuclei (AGNs) are among most powerful astrophysical sources in the Universe with bolometric luminosities of $\sim 10^{43}$ to 10^{48} ergs/s. There is a supermassive Black hole at centre of every AGN. Matters around BH fall into it causing very high viscous heating in layers bteween plasma in the process. Upto about 40% of mass can get converted to equivalent amount of energy in this process known as accretion. AGN's emissions are observed in a very broad range of spectrum, right from radio to high energy gamma ray frequency. Additionally these are also sources of variable nature with variability time scale ranging from minutes to days or longer. AGN flares with rapid variability owe its origin to a plethora of rich physics happening out there in the near accretion region having an expanse of mostly 20-30 r_G right from the event-horizon.
Thin accretion disk with various configuration of magnetic field topology threading it can potentially originate rapid variability. Magnetic reconnection is a potential mechanism to produce high energy particles carrying plasmoids.
SEDs from this kind of sources shows two humps. The lower energy hump is from Synchrotron radiation originated by gyration of relativistic particles around magnetic field lines. Inverse Compton process in which lower energy seed photons are upscattered to higher energy ones causes second higher energy hump.
As the lengthscales we are interested in are not resolvable with our state-of-the-art observing facilities the exact mechanism of extracting black hole spin energy to produce strong collimated relativistic jet and non-thermal radiation close to BH is still sensitively dependent on theoretical models. One way to explore these theoretical predictions are performing numerical simulations with desired setup. Several authors have reported results of high resolution performed with different initial setup. Armed with computing prowess of recent era super high-resolution simulations are possible exploring intricate physics happening very near to black hole.
Small scale physics like instabilities, current sheet formations, resistivity operating between layers of plasma, magnetic stress, tension etc play relatively superior role in producing large scale effects which are observable with telescope facilities at our disposal. Magnetorotational instability plays a major role in conserving angular momentum of accreting matters to produce relativistic jet in Blandford-Znajek(BZ) [3] process and to produce disk-winds in Blandford-Payne(BP)[2] mechanism. These two models are well accpted for extracting BH rotational energy in an electromagnetic fashion which was originally proposed for pulsars.
Current sheet formation and eventual magnetic reconnection is a potential mechanism to produce small islands of magnetic field lines carrying high energy particles. These

plasmoids can explain short timescale variability from AGN and flares. The timescale is less than the light-crossing time-scale of of event horizon constraining the emitting region to be of the order of a Schwarzschild radius. Plasmoids formed in a resistive accretion disk can have this lengthscale and energy to explain such observations. A single magnetic reconnection event can produce a chain of plasmoids, i.e. a series of plasmoids having different sizes and bulk Lorentz factor *(Shibata & Tanuma 2001[34]; Huang & Bhattacharjee 2012[14]; Uzdensky et al. 2010[39]; Loureiro et al. 2012[16]; Sironi et al. 2016.[36])* Several works (e.g *Petropoulou et al (2018)[26]*) have explored various physical processes (e.g. acceleration, growth, merger etc.) that determines the size and momentum distributions of the plasmoids in a chain using a Monte Carlo simulation approach revealing a significant match with simulation results using PIC models. In an area spanning up to a size of ~ 0.2 of the reconnection layer's half length, the size distribution of plasmoids was discovered to be a power-law with negative index. L (measured in the rest frame of jet). The magnetization σ has just a little influence on slope. A recent 2D relativistic reconnection event simulation revealed that an observer at a distance receives nonthermal radiation from a huge number of plasmoids of various sizes and Doppler factors that share a single layer at any given time. Mildly relativistically moving plasmoids can contribute to slowly-varying component of light curve while the fast moving plasmoids can explain the rapid flare variabilities in such environments*(Christie,2019b).*

1.1 Accretion Disk around Black hole

Plasma particles around black hole rotate in sub-Keplerian orbit to eventually fall into Black hole. Radial velocity of these particles are very small compared to their relativistic azimuthal velocity.Disk is result of angular momentum possessed by particles falling in. They cannot simply fall into BH in a straight line as spacetime around the compact object is curved due to intense gravity of it. The curved spacetime around a rotating BH is described by Kerr metric (due to Roy Kerr). To an outside observer geodesic in a curved spacetime often looks distorted. Accretion disk is where most of particles lose their angular momentum and energy due to friction in adjacent layer. Gravitational energy is also released in accretion process.Total energy released in accretion process is divided in two parts with one boosting kinetic energy of particles and other emitting out from disk surface in form of thermal energy. Mostly thermal radiation spectrum from accretion disk is dependent upon mass accretion rate. In year 1973(*Shakura & Sunyaev* [33]) gave model of stable thin accretion disk structure which has been used most widely in subsequent works. In same year *Novikov and Thorne* [21] formulated the stable disk structure in strong gravity regime considering general relativistic effects. Novikov-Thorne disk model has been derived mathematically based on a number of assumptions including vanishing of r -ϕ component of Maxwellian stress at radius of the Innermost Stable Circular Orbit (ISCO). This general relativistic disk has a density profile decaying in off equatorial coordinate direction with maximum at equatorial plane. Several previous works (e.g. *Penna et al,2010*) have shown a lower deviation (~3%) from NT model through GRMHD simulations. In our case NT disk density profile is taken as initial setup which is in vertical hydrodynamic equilibrium in GRMHD framework.

- **Inner Disk Region**
  Regions from event horizon to tens of Schwarschild radii can be called as near accretion region. This is region of high magnetisation(σ) which essentially is ratio

of magnetic energy to mass-energy)($\frac{B^2}{\rho}$). Current density in azimuthal direction is also high here. Due to turbulent nature of magnetic field there current sheet formation and plasmoid chain production thereafter is possible in this region with plasmoids of varying size and Lorentz factor. Resistivity , magnetisation and rest mass density in this region are primary factors to initiate magnetic reconnection and plasmoid formation.Change of magnetic field topology from poloidal to sufficiently toroidal can produce plasmoids of shape far from spherical and affect its orientation also. The energy distribution in processes happening in near accretion region can energize plasmoids essentially rendering them unbounded from from pull of gravity of Black hole.
This region due to high turbulence in magnetic field ,MRI(magnetorotational instability) can determine on accretion rate thereby making it RIAF(Radiatively Inefficient Accretio Flow) or ADAF(Advection Dominated Accretion Flow). At super-Eddington accretion rate disk region become optically thick and hot producing ADAF.When the magnetic pressure equals gas pressure accretion process could halt making it a MAD(Magnetically Arrested Disk). BP Disk winds and BZ jet are also products of mass flux rate. Figure shows a schematic diagram of the system.

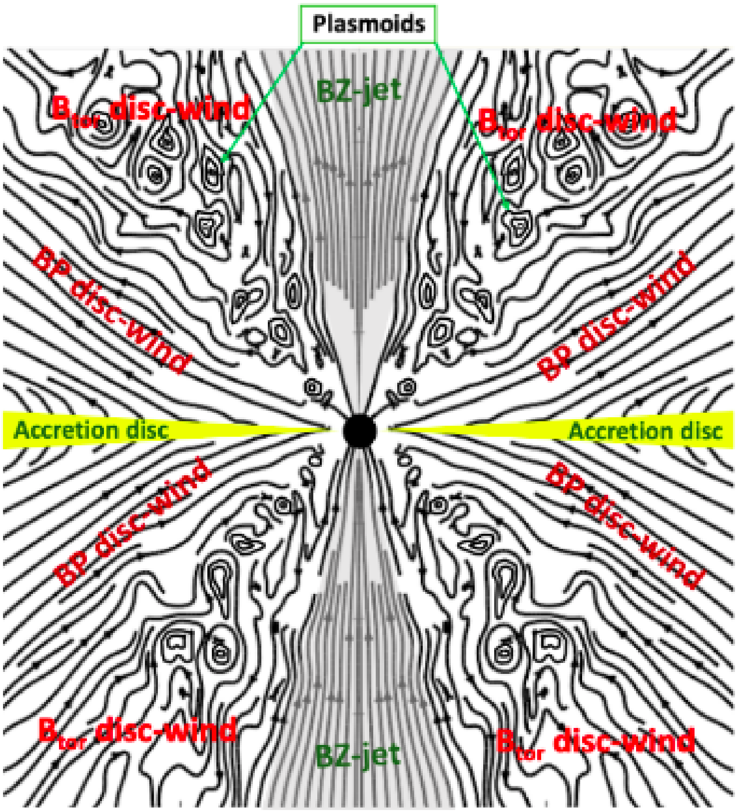

Figure 1.1: Schematic diagram BH-disk system(*Dihingia et al 2021*).

- **AGN Flares**

  Flares are observationally detectable order of magnitude increase in flux at certain frequency due to episodic burst of energy through some mechanism. From near central BH of AGN flares have been observed in many observational studies.Flares are observationally associated with an increase of almost two orders of magnitude

in the typical NIR emission *(Ponti et al. 2017[28];Do et al. 2019)*, but such an increase is difficult to be accounted for in terms of a significant change in the accretion flow *(Ressler et al. 2018[30])*. Recently *GRAVITY collaboration et al* in 2018 detected orbital motion originated at inner edge of accretion disk of Sgr A*. Sgr A* is a test-bed for many such events in high gravity regime due to proximity for our observation. Moreover Blazars which are AGNs having its jet inclined to nominal angle or almost toward our line-of-sight have also been observed for its variability in recent studies. Fluctuations above the flux-average in a relatively shorter timescale have been observed even in high-energy part of electromagnetic spectrum. In recent observations using Cerenkov telescopes at very high energy, the flux-doubling period has been detected to be as short as a few minutes in blazar flare outbursts (100 GeV).(e.g. *Aharonian et al. 2007; Arlen et al. 2013; Albert et al. 2007* and the Fermi Large Area Telescope in 0.1-300 GeV range (LAT; *Aleksi ́c et al. 2011; Ackermann et al. 2016; Shukla et al. 2018 [35]*). The TeV flares duration were observed for two Blazars namely Mrk 501 and PKS 2155–304 and as per inferred mass of central supermassive black hole(10^9 solar mass) variability of a few minutes is far less than light crossing timescale of event horizon. On top of that escape of TeV photons implies avoidance of pair creation in soft surrounding radiation field which practically indicated bulk Lorentz factor of $\Gamma_{\rm em} \geq 50$ essentially meaning a compact region in Blazar jet. *Meyer et al.2019* [17] have analyzed the brightest γ-ray flares of a number of selective flat spectrum radio quasars (FSRQs) during 10 years of Fermi-LAT data. [17] . High energy flares are also thought to energize particles to intense ultrahigh energy cosmic ray. Evidence for subhour timescales (as short as minutes) has been reported for two FSRQs in the sample (3C 279 and CTA 102) at a $\sim 2\sigma$ post-trial significance.
Short timescale γ-ray flares from AGN are of particular importance for they can be used to constrain production mechanism and underlying physical processes(e.g. *Giannios et al. 2010; Nalewajko et al. 2011; Narayan & Piran 2012; Aharonian et al. 2017; Petropoulou et al. 2017[27]*). On the other hand,the multiwavelength simultaneous observation of variability and study of their correlation can provide valuable insight about physical mechanism and reprocessing of seed photons in those environments(e.g. *Chatterjee et al*,2021 [8]).

1.2 Motivation

1.2.1 Short timescale variability of AGN

To explain TeV flares at subhour timescale from Blazars various models have been proposed. Essentially the bulk Loentz factor and physical size of emitting region are two most important parameters that constrain models for emission in this scenario. As TeV photons is able to escape from emitting region without pair creation it is natural to assume a comparatively larger Lorentz factor($\geq$50) of bulk of jet.But in reality patterns in jet were observed to move with moderate Lorentz factor of $\Gamma_{\rm j} \sim$10. To explain this apparent contradiction some uthors have proposed significant deceleration of compact emitting region of jet on sub-pc scale by some processes like radiative feedback on spine or sheath configuation (*Ghisellini, Tavecchio & Chiaberge 2005[12]; Tavecchio & Ghisellini 2008[38]*). Others have suggested small opening angle of jet at positions to slow down prominent radio knots (*Gopal-Krishna, Dhurde & Wiita 2004 ; Gopal-Krishna et* *al. 2007*). *Giannios et al* [13] in 2009 has proposed **'Jets-in-jet-model'** where they have taken a compact blob of plasma moving at some angle to radial direction where the characteristic Lorentz factor of blob is much greater than jet Lorentz factor provided motions in jet are relativistic. In a Poynting-Flux dominated flow this kind of fast motion is possible. Assuming occasional magnetic reconnection in jet one can figure out the energetics as follows. In a Poynting Flux dominated accretion flow current driven instabilities play a major role in dissipation process of immense magnetic energy through magnetic reconnection. In this picture whilw highly magnetized material is advected to reconnection region part of magnetic energy is converted to boost kinetic energy of the outflowing matter particles known as emitting blob and part of it is expended in heating materials to relativistic temperature. Same situation conducive to magnetic reconnec-

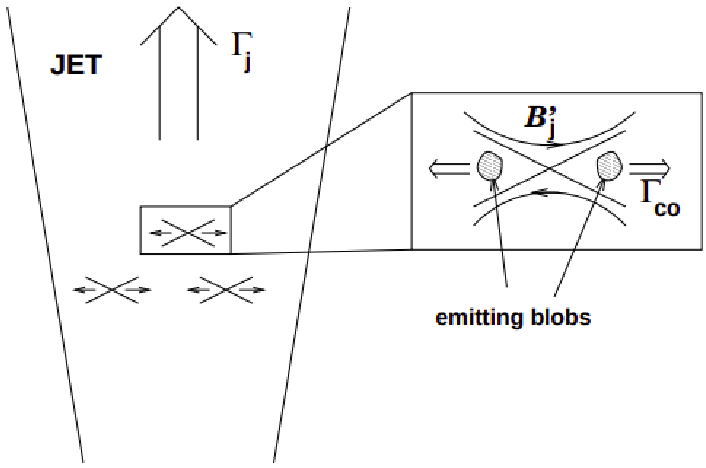

Figure 1.2: Figure demonstrates schematically the configuration and mechanism of the 'Jets-in-jet' model (*Giannios et al 2009*).

tion event can be numerically realized in a scenario where the sense of outer spiraling of helical magnetic field lines is opposite to the inner spiraling magnetic field in apex region of jet. Through synthetic emission map different topology of magnetic field and shear velocity between plasma column inside a jet have been explored in 3D simulation in*Borse et al[5]*. Due to Kelvin-Helmholtz instability in plasma column shocks are formed in localized region which can reaccelerate and re-energize a local population of electrons with static flat spectral slope to higher energy only to cause a second Synchrotron hump to appear in synthetic emission map. This secondary poulations maximum energy can go upto ν=10^{21}Hz that can easily upscatter CMB photons to higher TeV photon thereby producing a flare.
However,long current sheet due to instability and topology of accreting magnetic flux can also form chains of plasmoids.*Nathanail et al*[20] in 2020 showed through 2D ideal GRMHD simulation that an Fishbone-Moncreif(FMTorus) torus with poloidal magnetic loops with alternating polarity around a accreting Kerr BH can produce chains of unbounded plasmoids. A quantity called Bernoulli constant which is given by hu_t where h is scpecific enthalpy of accreting matters and u_t is temporal component of fluid four-velocity has been used to find whether plasmoids are unbounded.

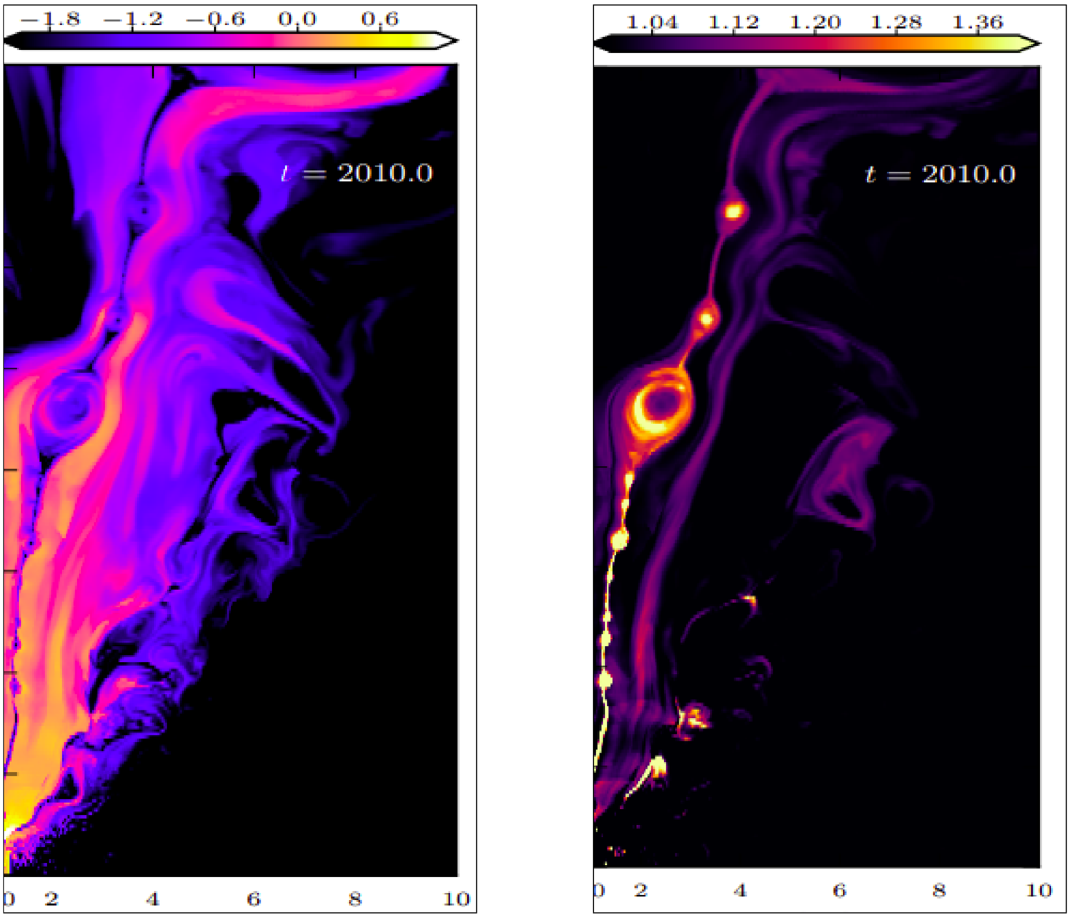

Figure 1.3: Figure on the left shows logarithmic plot of σ at time $t = 2010$ in code units. Figure on the right is a plot of Bernoulli constant showing chain of plasmoids (*Nathanail et al 2020*).

Rapid alternation of toroidal magnetic polarity embedded in torus helps form current sheets. Also in region where torus mass is high and magnetization is low plasmoid formation is hindered. Hence toward polar region where rest mass density is low and exists a significant gradient of magnetization plsmoid chain formation is more pronounced. Ideal GRMHD simulation supposed to produce large numbers of plasmoids in each magnetic reconnection event than resistive MHD. Resistivity in plasma layers is efficient in destroying closed loop topology of magnetic field lines formed in reconnection.
Plasmoids formed in magnetic reconnection event can carry a population of highly energetic particles. Given a reliable model of non-thermal emission from such population of particles, the detailed energy budget can be estimated to demonstrate the short timescale high flux variability of AGN flares in general.

1.2.2 Magnetic Hair

The original "No hair conjecture" on black hole states that all stationary, asymptotically flat black hole spacetime geometry can be sufficiently described by its mass, spin and electric charge. Later, it was demonstrated that on a lightcrossing timescale, any field with zero rest mass and arbitrary integer spin will be radiated away from BH. However *Bransgrove et al*[6] in a very recent letter(2021) argued in presence of electrically conductive plasma surrounding BH, losing magnetic energy is not easily prescribable which

magnetized BH possesses from its magnetized progenitor.Only way to loose this "Magnetic Hair" is by changing its topology thereby reconnecting and forming outbound loops of magnetic field lines. Hence unbounded plasmoid formation in BH magnetosphere is a theoretical obligation. To test classical no hair theorem they took a magnetized Neutron Star (NS) with already accreting plasma just after it undergoes collapse and forms a black hole.
They reported GRRMHD (general-relativistic resistive magnetohydrodynamics) and GRPIC (general-relativistic particle-in-cell) are converging for first time to produce correct reconnection physics. In vacuum the curl of magnetic field is either radiated away or swallowed by BH but in presence of plasma this balding process slows down driving current. Plasma inside ergosphere is co-rotated with BH due to strong frame-dragging (*Yakov & Itin, 2008*)[40]. This is reason of conversion of purely poloidal magnetic field into toroidal magnetic field in the inner disk region, thereby creating instabilities. In GRRMHD simulation using `BHAC` the uniform diffusivity is set to 10^{-5} to favour plasmoid instability. The plasma is electron-positron pair plasma in this case and the diffusivity η is primarily due to the coulombic collision of the pairs. Plasma is nearly force-free for a minimum density level is set in this simulation.
A general relativistic particle-in-cell (PIC) code named `Zeltron` is used to simulate kinetic plasma. Simultaneously, the equations of motion for pair plasma particles and Maxwell's equation are solved.

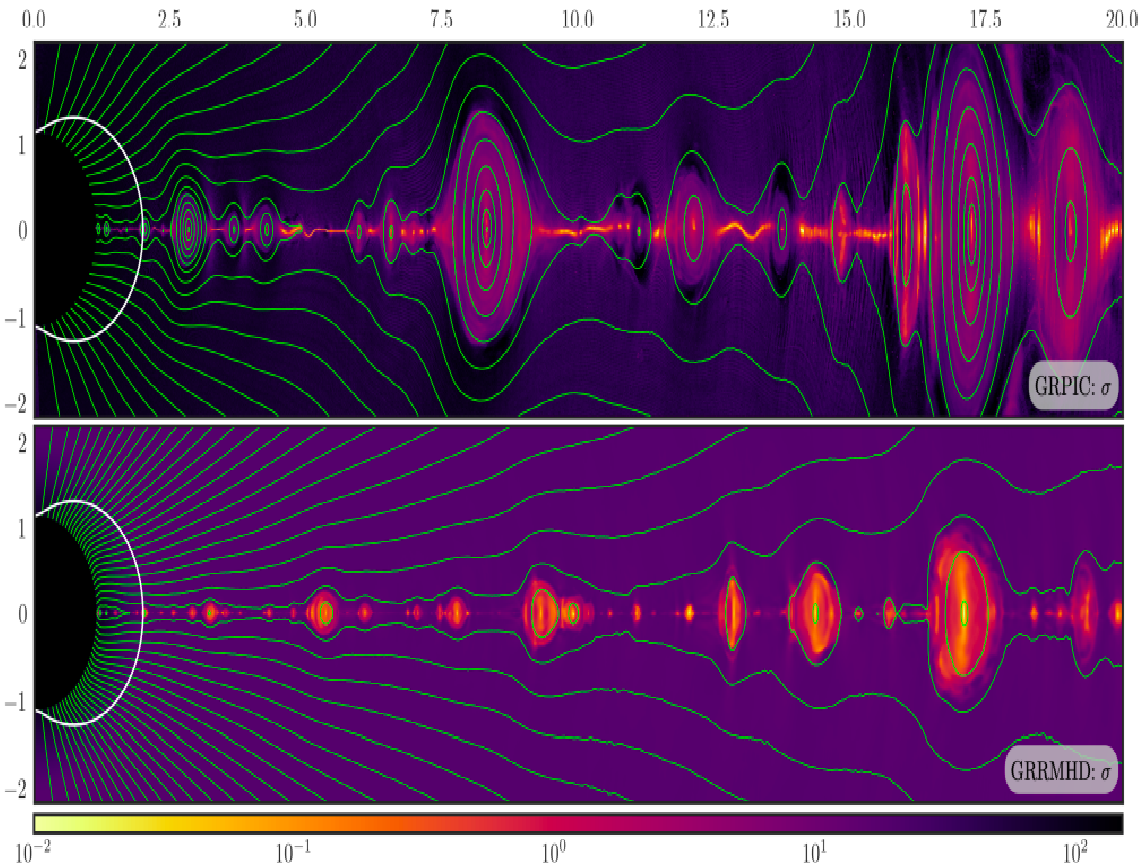

Figure 1.4: GRPIC (UP) and GRRMHD(DOWN) simlation showing magnetization and plasmoids formed in magnetic reconnection. Green lines are field lines of poloidal magnetic field. *Branshgrove et al 2021.*

The value of the diffusivity η is changed constantly in GRPIC simulation due to the fact that the value is calculated from first principle (non-uniformity in the electronic pressure tensor) at different time steps. Hence, the reconnection rate differs from each other in the two cases. In course of the simulation when the current sheet is sufficiently thin, the tearing mode instability develops and forms chains of plasmoids with varying sizes through the process of magnetic reconnection. Reconnection kicks in at the static limit (surface of the ergosphere), and gradually the entire current sheet is involved in the process. It is observed that the plasmoids formed inside the static limit moves with lower velocity and falls into the black hole, whereas, those formed outside escapes the system. However, episodically some plasmoids formed inside the limit are significantly energized to escape the system. Hence statistics of plasmoids formed near BH regarding their size and energy distribution is necessary. From that knowledge with a simplistic model of non-thermal radiation from reconnection heated particles, we produce a consistent luminosity of the plasmoids, which, over the entire flux rising and decaying time scale, account for the total energy budget of each observed flare. In the present work we progress toward the investigation and present our results obtained.

Chapter 2

Numerically Modeling Accretion Disk

2.1 BHAC

The **B**lack **H**ole **A**ccretion **C**ode or BHAC is publicly available GRMHD code written in language of Fortran . It was developed by Porth et al(*Porth, O., Olivares, H., Mizuno, Y., Younsi, Z., Rezzolla, L., Moscibrodzka, M., Falcke, H., Kramer, M. (2017)*[29]. and *Olivares, H., Porth, O., Davelaar, J., Most, E. R., Fromm, C. M., Mizuno, Y., Younsi, Z., Rezzolla, L. (2019))[22]*. BHAC is designed to solve ideal as well as resistive GRMHD equations in arbitrary spacetime. It exploits Adaptive Mesh Refinement (AMR) technique in a block-by-block basis. The transition of physics module of SRMHD code MPI-AMRVAC to GRMHD BHAC is introduction of 3+1 split of spacetime. The three ideal conservation equations of GRMHD are

$$\nabla_\mu(\rho u^\mu) = 0, \tag{2.1}$$

$$\nabla_\mu T^{\mu\nu} = 0, \tag{2.2}$$

$$\nabla^*_\mu F^{\mu\nu} = 0. \tag{2.3}$$

First is mass conservation , second implies conservation of stress-energy tensor that also includes the covariant specific magnetic energy density (b^2/ρ) in the total enthalpy and the third is dual of Faraday tensor (Source-free Maxwell's equations).By virtue of spatial projection operator these three equations are decomposed into spatial and temporal components.

Ampere's law (i.e., for the evolution of the electric field) has to be solved alongside the ideal GRMHD equations to incorporate resistivity η in ideal formulation. Assuming $\vec{E} = -\vec{v} \times \vec{B} + \eta\vec{J}$ would change induction equation (Faraday's law)too which should be taken into account.

To control the $\vec{\nabla} \cdot \vec{B} = 0$ constraint on AMR grids BHAC employs a constraint dampening approach. For hydrodynamic variables, a cell-centered Flux-interpolated Constrained Transport (FCT) is consistent with a finite volume scheme.The CT systems try to keep the sum of magnetic fluxes through all surfaces enclosing a cell to zero at machine precision, and hence the divergence of the magnetic field inside the cell (in the continuous limit).

To increase flexibility of BHAC to be able to solve BH accretion in arbitrary spacetime several coordinate systems are available for describing metric components.Cartesian, spherical, modified Kerr-schild, Rezzolla and Zhidenko parametrization are some of them.

Several temporal schemes like third-order Runge-Kutta (RK) RK3, strong-stability preserving s-step, pth-order RK schemes SSPRK(s,p)are available for temporal update(e.g. SSPRK(4,3), SSPRK(5,4)).

BHAC employs adaptive mesh refinement technique thereby increasing resolution in area of interest and helping in convergence. Essentially coarsening or refining of grid in BHAC is decided upon estimating whether local error exceeds a user-set tolerence level.

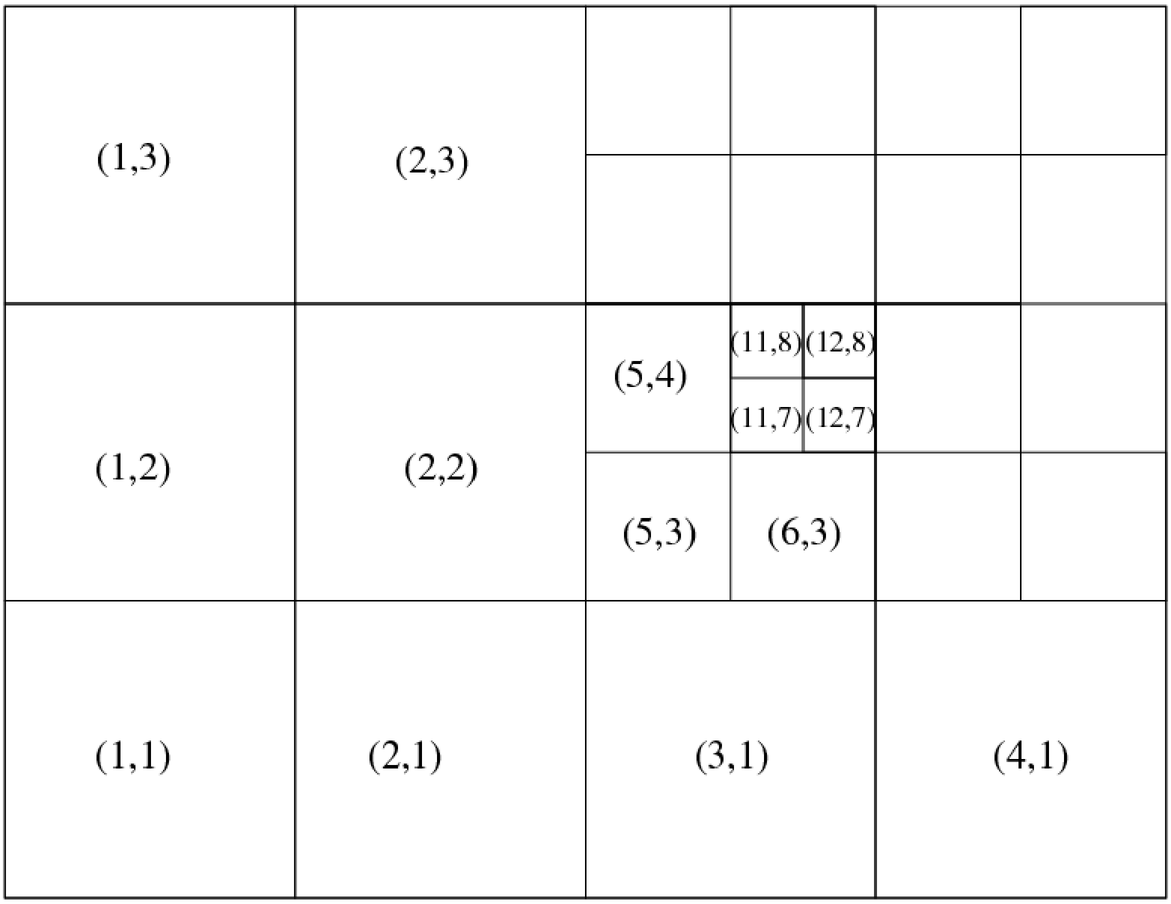

Figure 2.1: Adaptive mesh refinement:Figure shows a 2D hypothetical square grid with 4 blocks on level 1. Refinement has been activated in 4 out of these level 1 blocks to obtain level 2 grid blocks. The numbered tuples correctly locate the grid when one has AMR level knowledge as well.

2.2 Numerical Disk Setup

The thin accretion disk setup implies that equatorial plane of the coordinate system ($\theta = \frac{\pi}{2}$) is occupied by most of the dense fluid and the θ-component of four-velocity is absent (zero). Our disk is set up in BHAC using the *Novikov & Thorne, 1973[21]* disk density profile in Boyer-Lindquist coordinate. The general density profile is given by

$$\rho = \rho_e exp(-\frac{\alpha^2 z^2}{H^2}); z = rcos(\theta).$$

where, ρ_e is calculated using NT algebraic formulationand H is scale height of accretion disk. The explicit form of H is given by, $H^2 = \frac{p_e r^3}{\rho_e F}$ following (*Peitz & Appl 1997[25]*

and *Riffert & Herold 1995[32]*). The quantities p_e and ρ_e are the equatorial pressure and density of the disk and F is defined as $F = \gamma_\phi^2 \frac{(a^2+r^2)^2+2a^2\Delta}{(a^2+r^2)^2-2a^2\Delta}$, where, γ_ϕ is the azimuthal Lorentz factor and $\Delta = r^2 - 2r + a^2$. To have a thin disk we set α=2.
The four velocity of to disk materials is given solving the standard four-velocity normalization and geodesic equation given by equations 2.4 and 2.5 respectively.

$$g^r_{tt}u^t u^t + 2g^r_{t\phi}u^t u^\phi + g^r_{\phi\phi}u^\phi u^\phi = -1, \tag{2.4}$$

$$u^t u^t \Gamma^r_{tt} + 2u^t u^\phi \Gamma^r_{t\phi} + u^\phi u^\phi \Gamma^r_{\phi\phi} = 0. \tag{2.5}$$

For better handling of the low-density environment in the vicinity of black hole, the following floor density model has been adopted in the code, $\rho_{flr} = \rho_{min} r^{-2}$ with $\rho_{min} = 10^{-5}$. Additionally, a maximum limit is also set on the values of bulk Lorentz factor, $\Gamma_{\max} = 20$. An inclined poloidal magnetic field profile is set following *Zanni et al 2007* with an explicit form of

$$A_\phi \propto (rsin(\theta))^{\frac{3}{4}} \frac{m^{\frac{5}{4}}}{(m^2 + tan^{-2}(\theta - \frac{\pi}{2}))^{\frac{5}{8}}},$$

where the inclination angle of the initial poloidal magnetic field lines and the amount of magnetic flux are determined by the parameter, m. We take m=0.1 for our simulation setup.The spin parameter of the BH is taken as $a = 0.9375$. For this spin parameter, the radius of Innermost stable circular orbit and the radius at which density attains a maximum value are obtained as $r_{ms} = 2.04424$ and $r_{max} = 2.97973$ respectively. Furthermore, we use a unit system with $G = M = c = 1$, where G, M, and c are the gravitational constant, mass of the black hole and speed of light in vacuum. Subsequently, any relevant length scale, time and angular momentum are manifested in terms of $\frac{GM}{c^2}$, $\frac{GM}{c^3}$ and $\frac{GM}{c}$ respectively. The plasma beta parameter is 10^3 to allow for a substantially strong magnetic field. We present here simulation result for two resistivities $\eta = 10^{-10}, \eta = 10^{-6}$. The initial setup is same for both the cases. Viscosity is introduced to this setup as non-ideal effect with *Shakura & Sunyaev* α prescription. Higher resistivity corresponds to a value greater than a Lundquist number against plasmoid instability. Hence lower resistive disk evolution is mainly focused here.

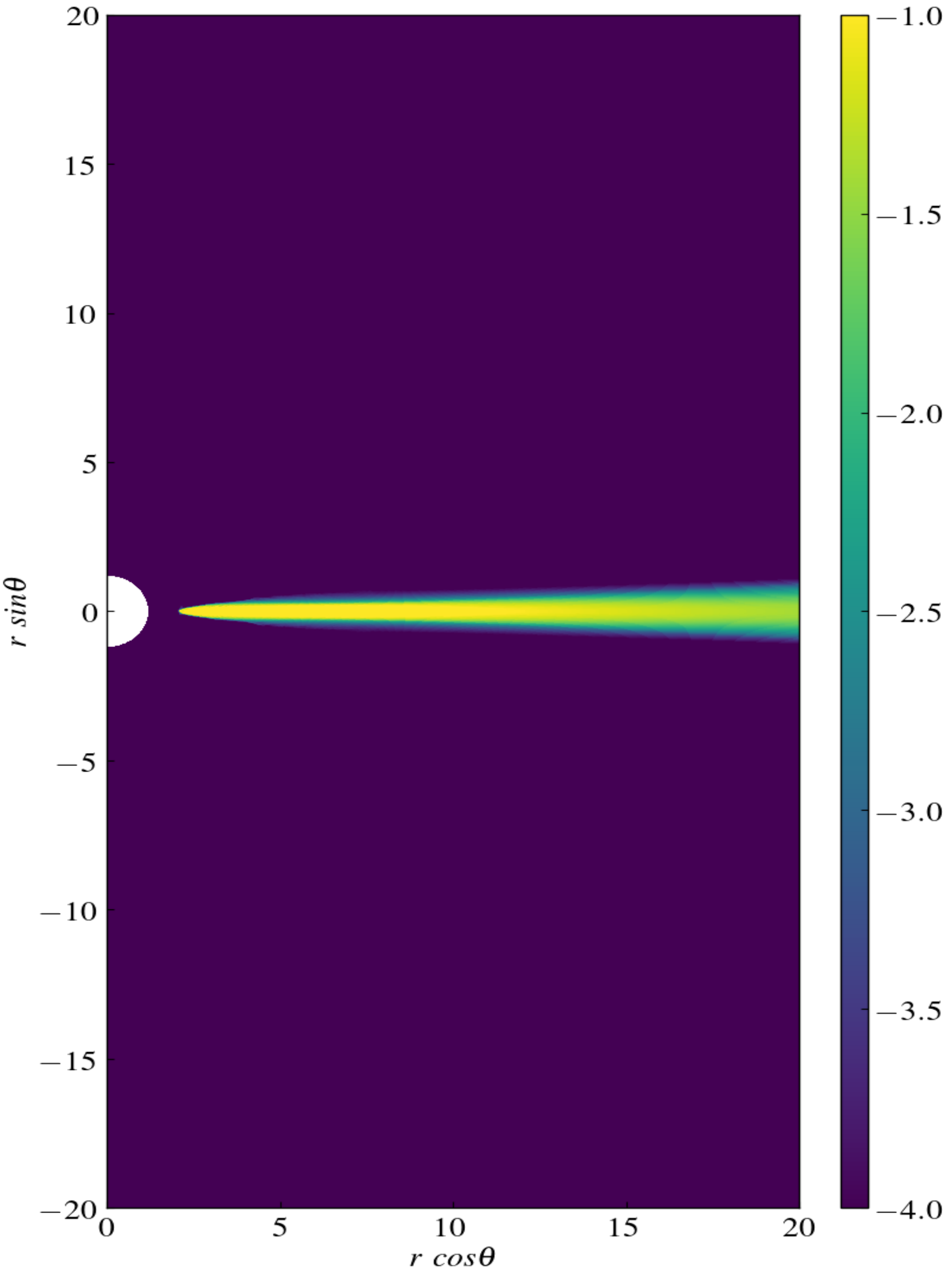

Figure 2.2: Logarithmic initial normalized density $(\frac{\rho}{\rho_{max}})$profile for accretion disk.

Chapter 3

Simulation Dynamical Result

3.1 Low resistive disk

The disk setup is evolved to a time $t = 2000$ with an effective resolution of 2048×1024. Evolution of disk density profile is shown here.

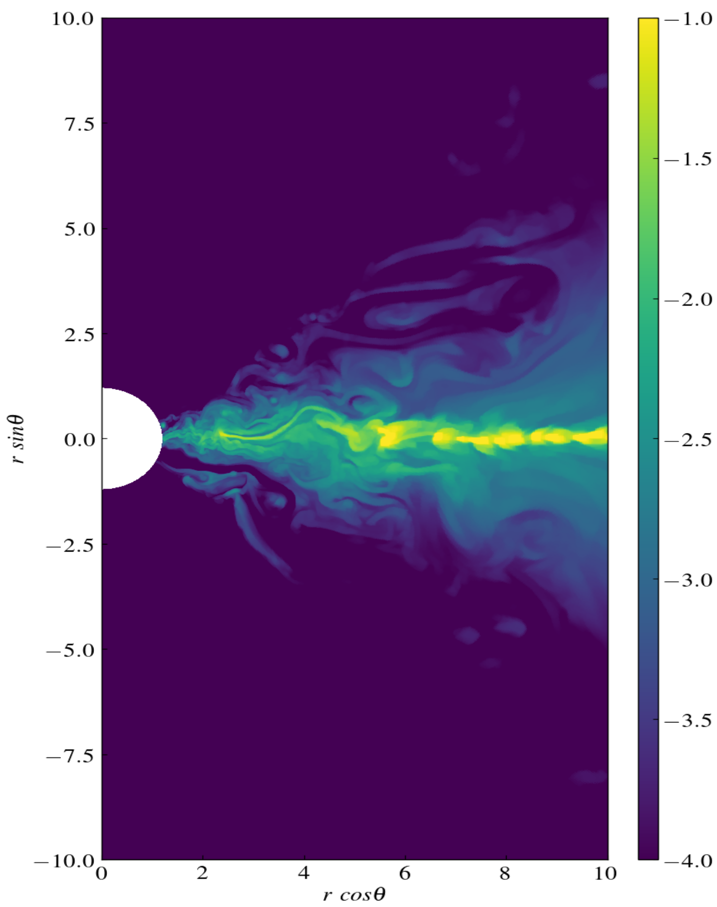

Figure 3.1: Logarithmic density profile normalized to its maximum value $(\frac{\rho}{\rho_{max}})$ profile for accretion disk at t=500.

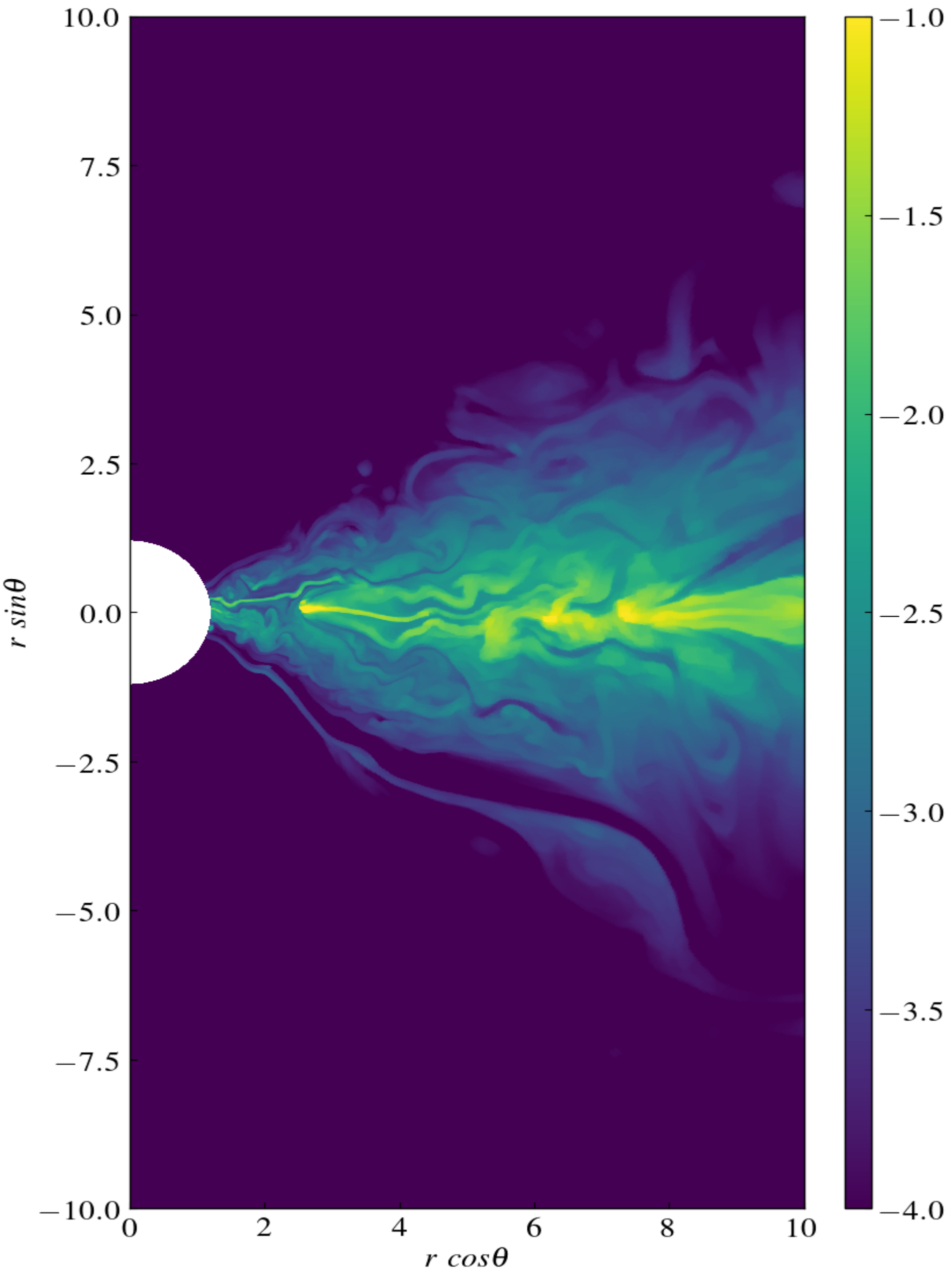

Figure 3.2: Logarithmic density profile normalized to its maximum value ($\frac{\rho}{\rho_{max}}$) for accretion disk at t=1000.

Disk rotation at onset of simulation transforms initially given poloidal magnetic field profile to a field toroidal component. This field is essential for transporting angular momentum and kicks in accretion of matter in an inside-out manner(*Dihingia et al 2021[11]*). This leads to subsequent disk-density profile with lower equatorial concentration and higher concentration at polar region(θ=$\frac{\pi}{2}$). It is important here to note that the tenuous plasma which is highly collimated and natuarally accumulates in the funnel region is not distinctly visible here due to lack of contrast in density in this comparatively smaller region from the central black hole. As the equatorial disk region is not force-free the materials are attached to the magnetic field lines. As the initial magnetic field lines are otherwise anchored to the disk, in the force-free region in the off equatorial plane the centrifugal force can take over the force of gravity to cause such BP disk wind [2].

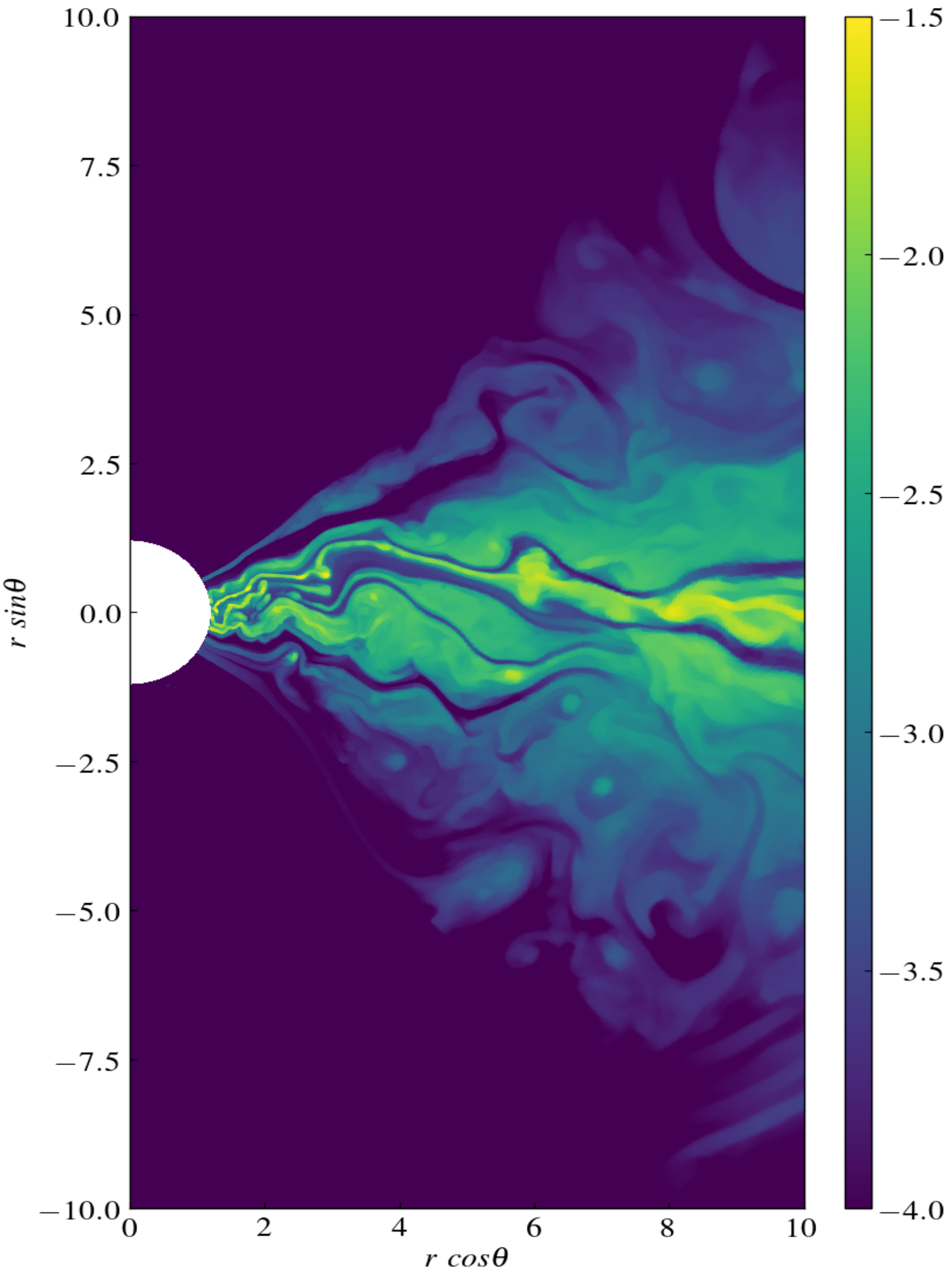

Figure 3.3: Logarithmic normalized density($\frac{\rho}{\rho_{max}}$) for accretion disk at time $t = 2000$.

In figure 3.3 , the low density filament like structures are very apparent. This could be the signatures of the episodic disruption of accretion flow due to developed magnetic pressure gradient while accumulating magnetic flux in the magnetospheric region. At t=2000 even with lower rate due to resistivity reconnection near BH produces macroscopic filamentary plasmoids. High mass and low magnetisation region correspond to low reconnection rate thereby producing small number of plasmoids.

To show disk wind from the setup we plot the Lorentz factor showing material outflow from disk away from BH. For localizing region with high magnetisation a plot of σ is also shown here at time t=2000.

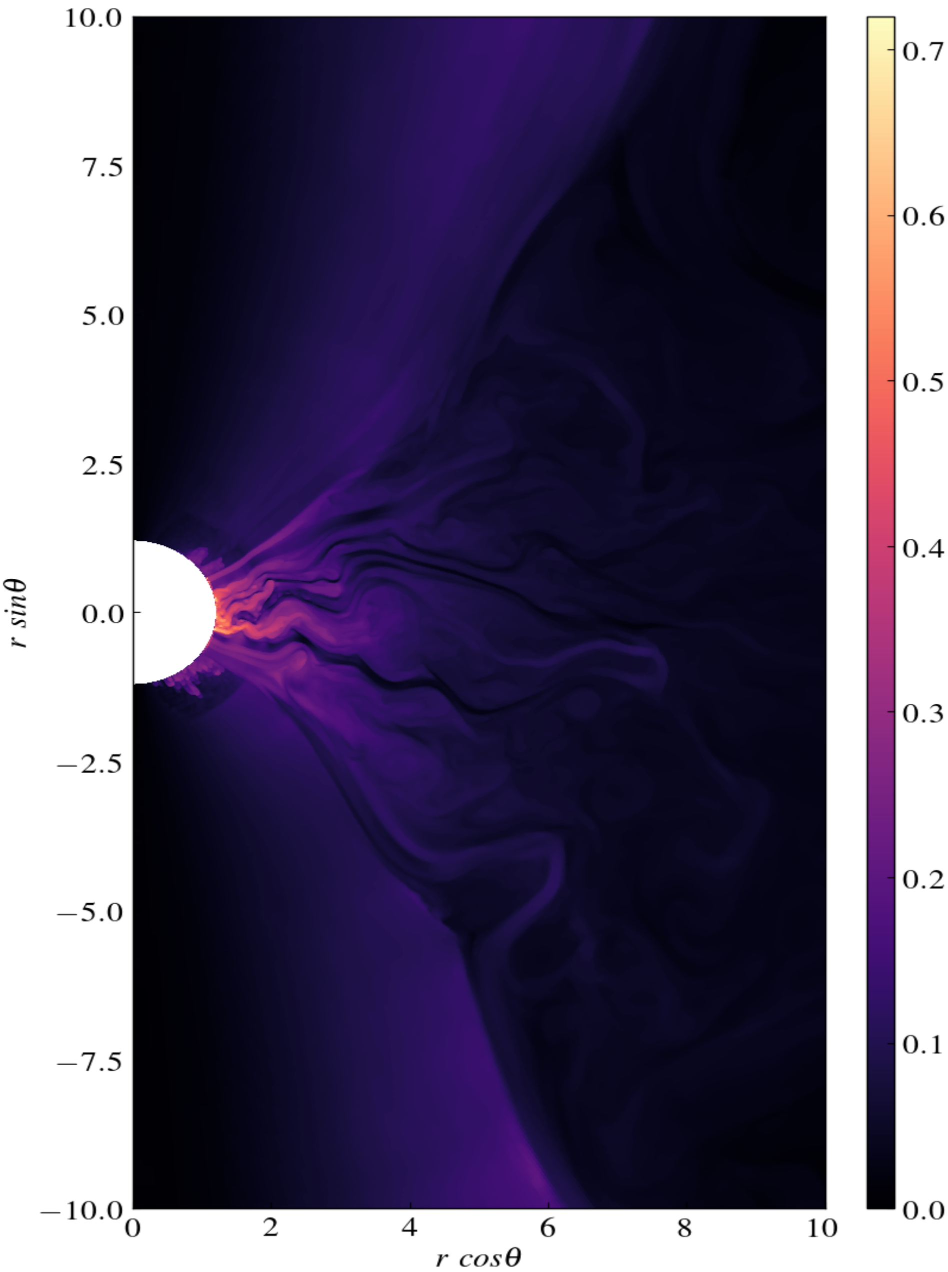

Figure 3.4: Logarithmic Lorentz factor profile for accretion disk at time t=2000.

Lorentz factor γ distribution shows significant matter from disk is directed to off-equatorial disk wind through action of magneto-centrifugal force in Blandford-Payne mechanism(1982). Plasmoids formed near BH are eventually advected to off-equatorial plane by wind. As can be seen in figure 3.4, the maximum Lorentz factor is achieved very close to the black hole. As the accretion process follows an inside-out flow profile, the back flow material self-consistently acquires a relativistic velocity and gets primarily channeled through the funnel region. Matter from equatorial disk subsequently fills out a large portion of numerical domain in this process.

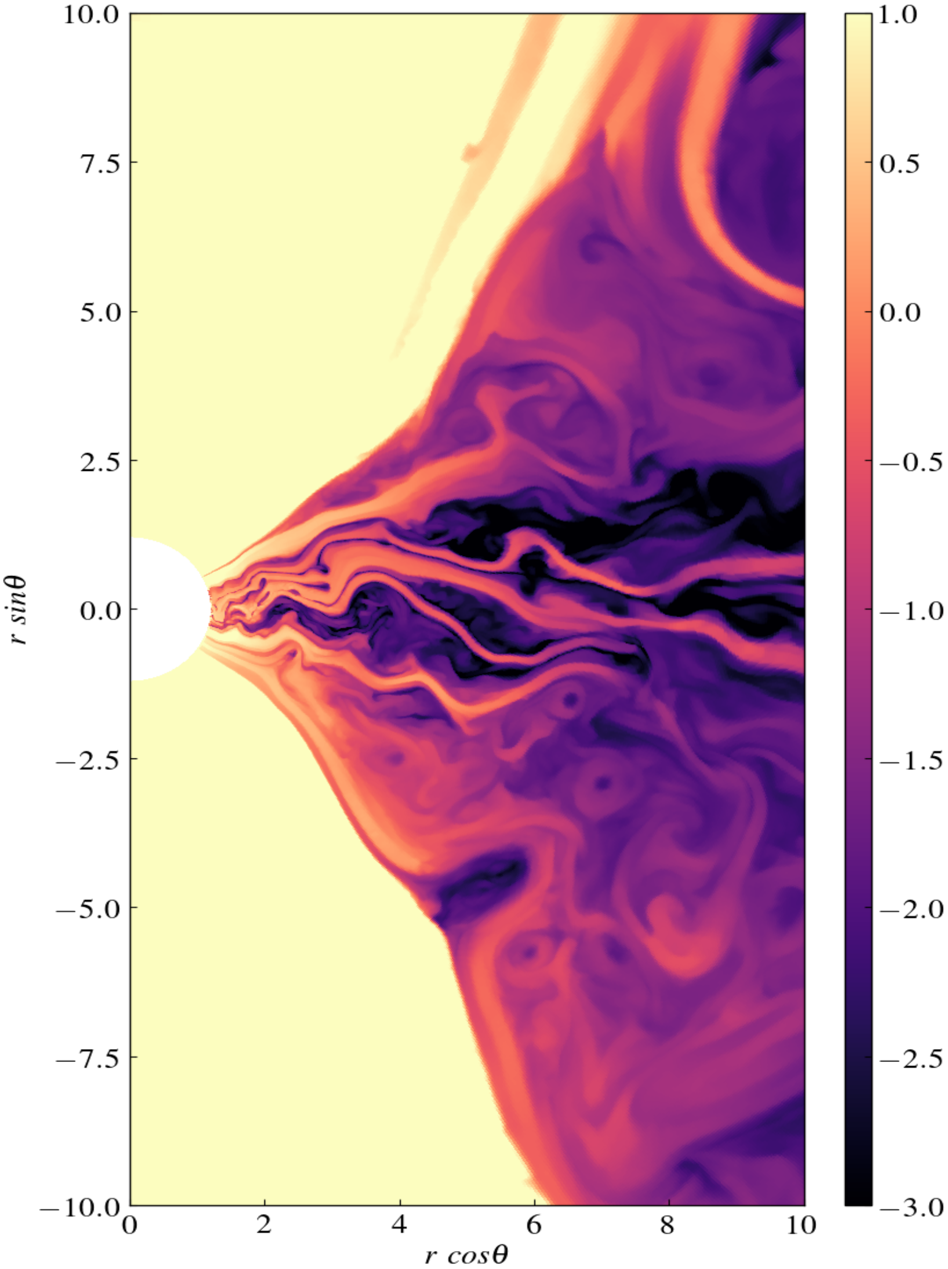

Figure 3.5: Logarithmic magnetisation (σ) profile for accretion disk at time t=2000.

Magnetisation σ distribution prominently shows formation of plasmoids in near accretion region. Almost spherical shaped plasmoids can be seen in lower-equatorial region. A significant increase in resistivity would distort shape of plasmoids formed in magnetic reconnection(*Nathanail et al 2021*). Plasmoid launching sites are concentrated near polar region and inside evolved disk.But lower mass density and higher magnetisation causes plasmoids of first kind to effectively carry higher energetic particles as outflow from disk.

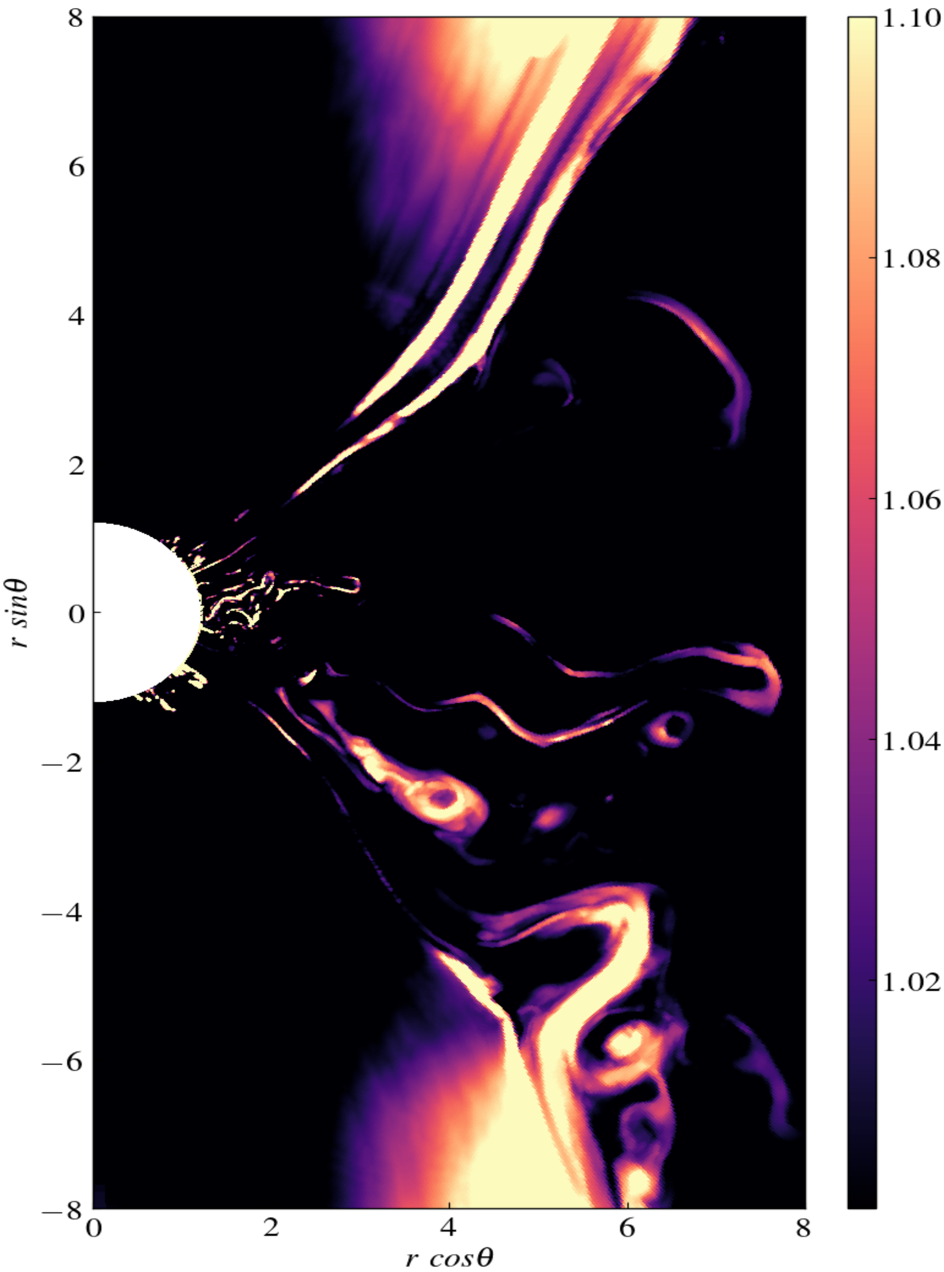

Figure 3.6: Distribution of hu_t above unit value for accretion disk at time t=2000 in regular scale.

Bernoulli criterion predicts whether a fluid element is gravitationally unbound . A fluid element is defined to be unbound if $hu_t \leq -1$.(*Rezolla & Zanotti 2013[31]*)Figure 3.6 shows in lower equatorial region gravitationally unbound regions which actually formed spheroidal plasmoids. Gravitationally unbound jet sheath can be observed near polar region.

3.2 Moderately Resistive Disk

Moderately rsistive disk with $\eta \sim 10^{-6}$ shows a some different type of features which demands for an independent investigation. Here we briefly present our result for highly resistive run results at a time t=2000.

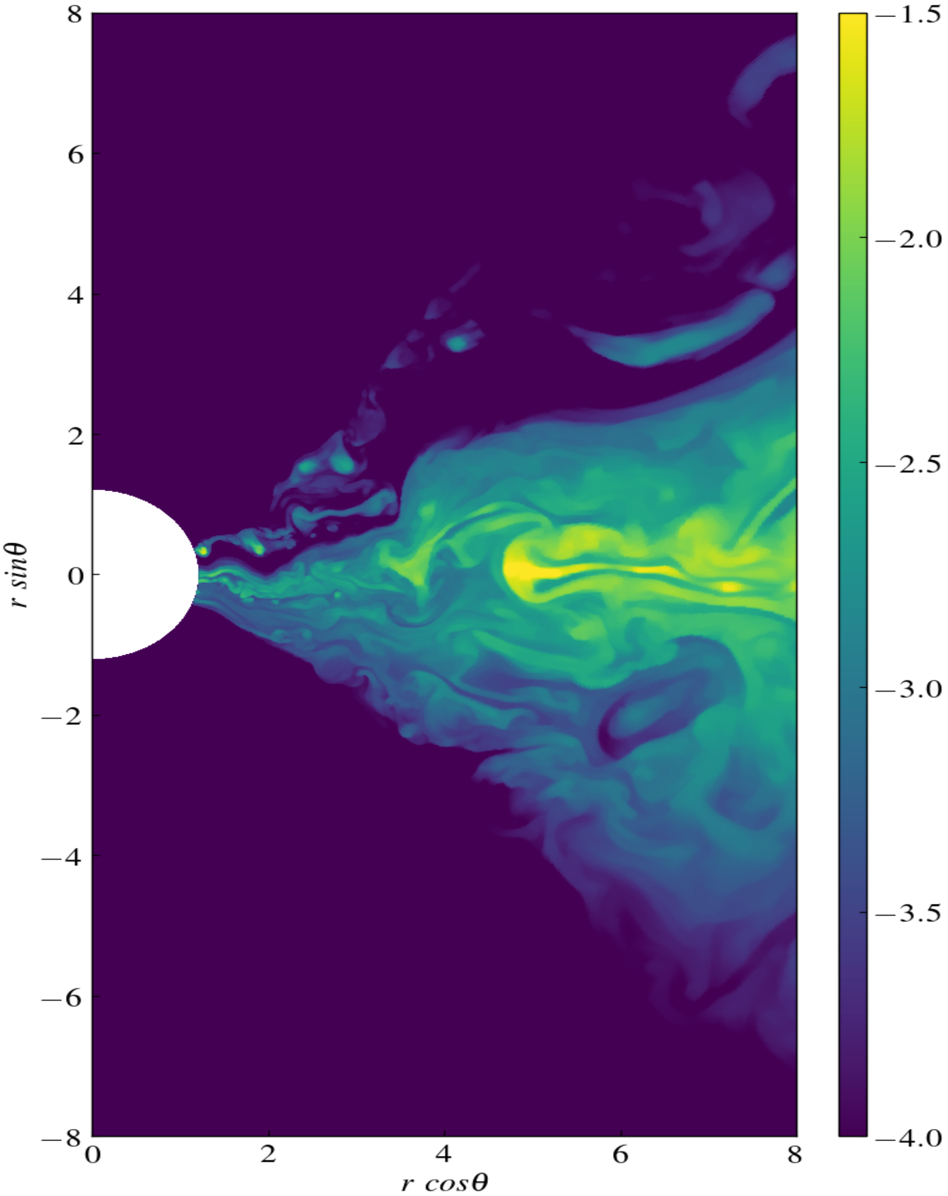

Figure 3.7: Logarithmic normalized density $(\frac{\rho}{\rho_{max}})$ profile for accretion disk at time t=2000.

The region in figure 3.7 is clearly divisible into three parts (a) the highly dense equatorial plane, (b) the off-equatorial low density region and (c) the jet funnel region with relatively lower density and ultra-relativistic outflow velocity. The highly relativistic region in funnel and disk wind in the off-equatorial region plays a crucial role in transporting angular momentum of the accreting matter of the disk around the BH.

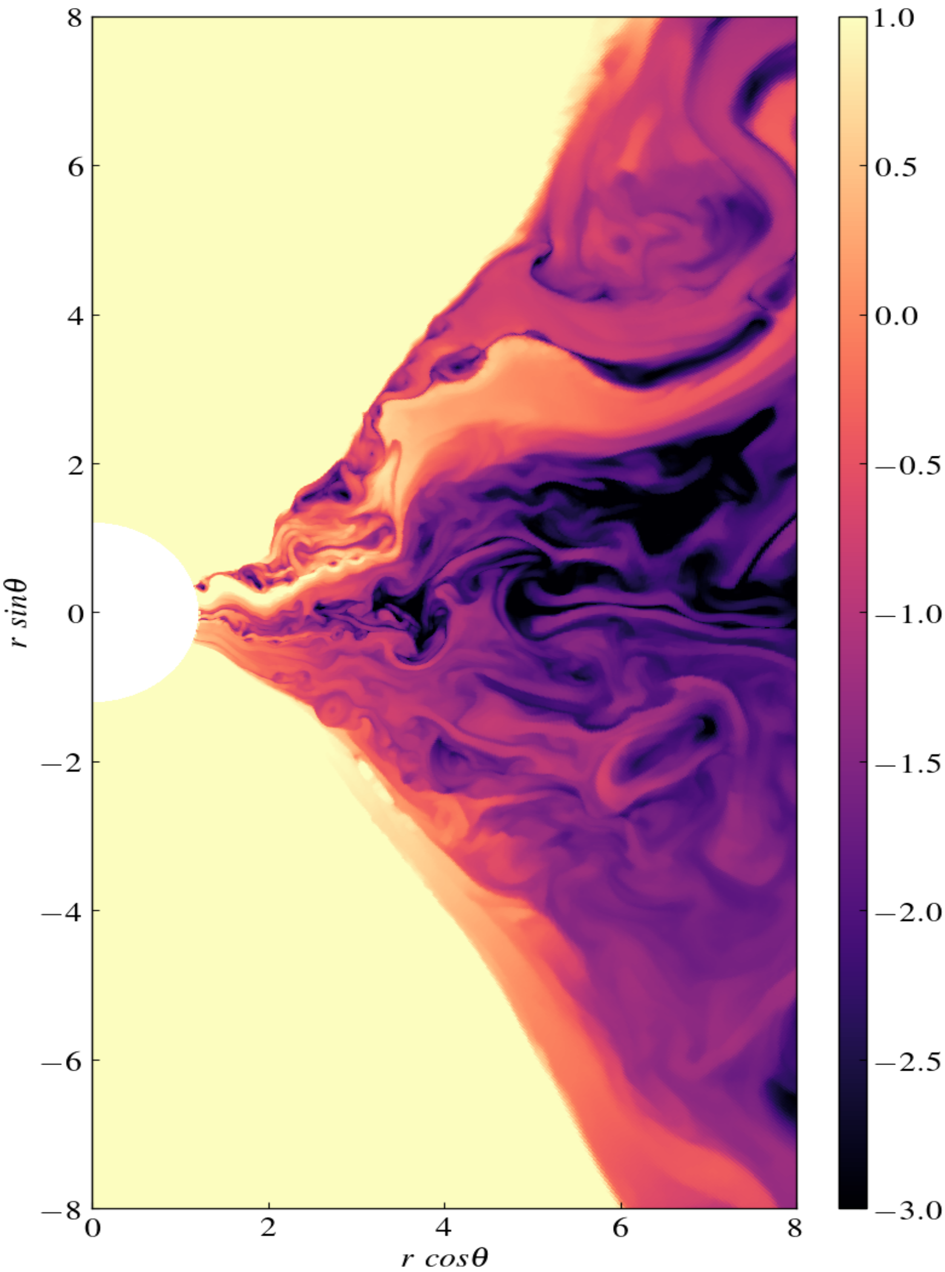

Figure 3.8: Logarithmic σ for moderately resistive disk at t=2000.

Magnetisation map here clearly shows a chain of palsmoids in upper half plane. A noticeable feature from previous and this image is where in the funnel sheath region a chain of plasmoids has been formed mass-density has been decreased there. This shows higher magnetisation and lower mass-density is essential for efficiency of magnetic reconnection. Hence in funnel sheath region having a strong gradient of magnetisation with low mass-density outflow of matter takes place efficiently through production of plasmoids by magnetic reconnection.

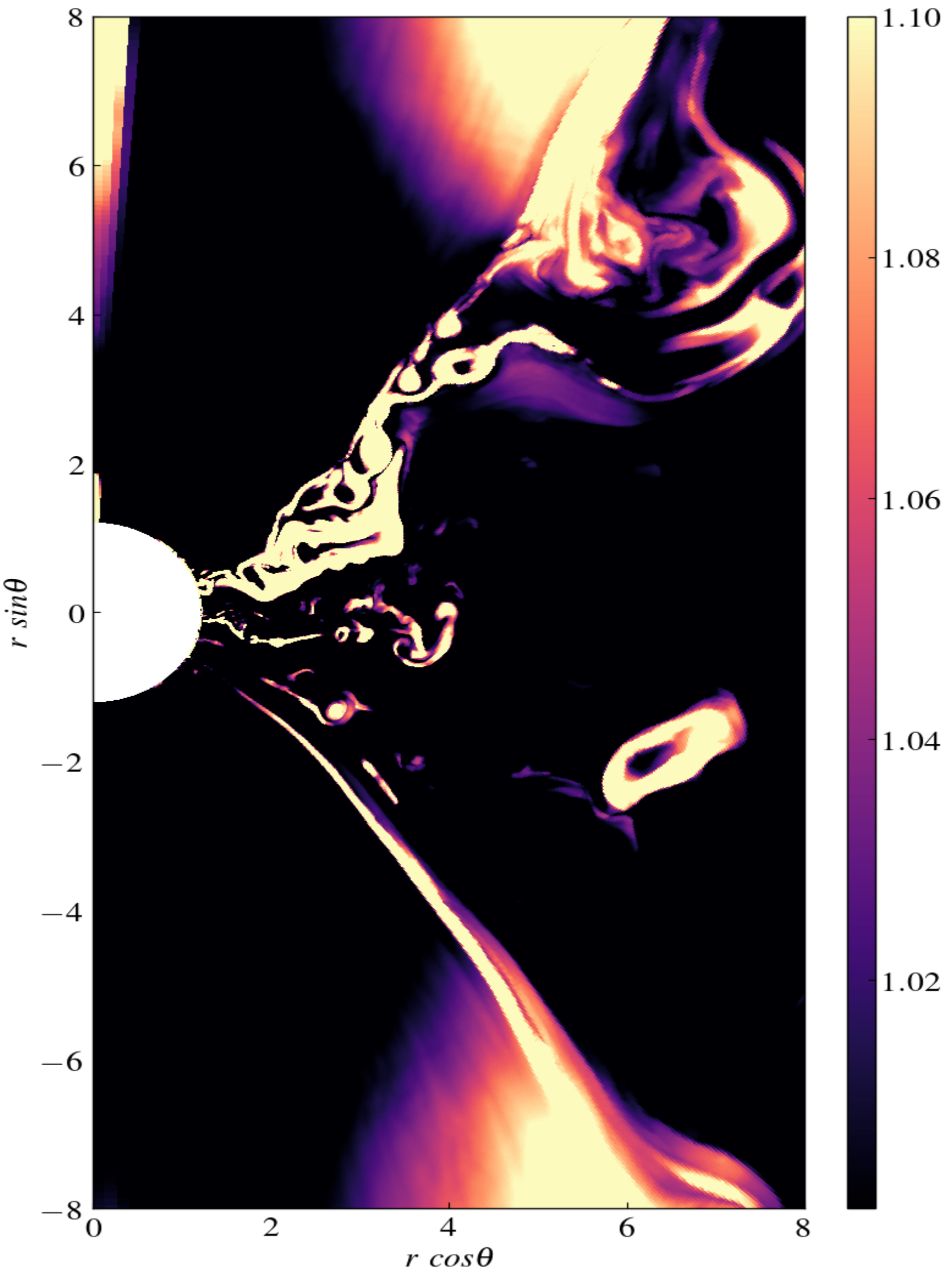

Figure 3.9: distribution of hu_t above unit value for moderately resistive disk setup at t=2000.

As can be seen from magnetization and hu_t distribution plasmoids do form in a moderately resistive disk.
Plasmoid detection can be done using edge detection algorithm to hu_t distribution while tracing the boundary and finding bright blobs can be done applying difference of gaussian method to hu_t distribution. A region with non-negligible magnetisation with large hu_t is searched from data to essentially find plasmoids that can contribute to subsequent flaring activity.(*Nathanail et al, 2020b, 2021*).

Chapter 4

Plasmoid Detection

4.1 Magnetic Reconnection

In a highly conductive plasma, magnetic reconnection is the process of breaking and rejoining opposite polarity magnetic field lines, converting magnetic energy to plasma kinetic and thermal energy. Reconnection of energy can release energy in an often explosive manner on a smaller scale, which can have global consequences. Electrons and ions gyrate and are tethered to magnetic field lines. When two magnetic field lines get closer to one another in a nearly collisionless plasma, a powerful current sheet can emerge. Even a vanishingly small resistance in a small volume can be essential in allowing particle diffusion and, as a result, modifying magnetic topology via magnetic reconnection.

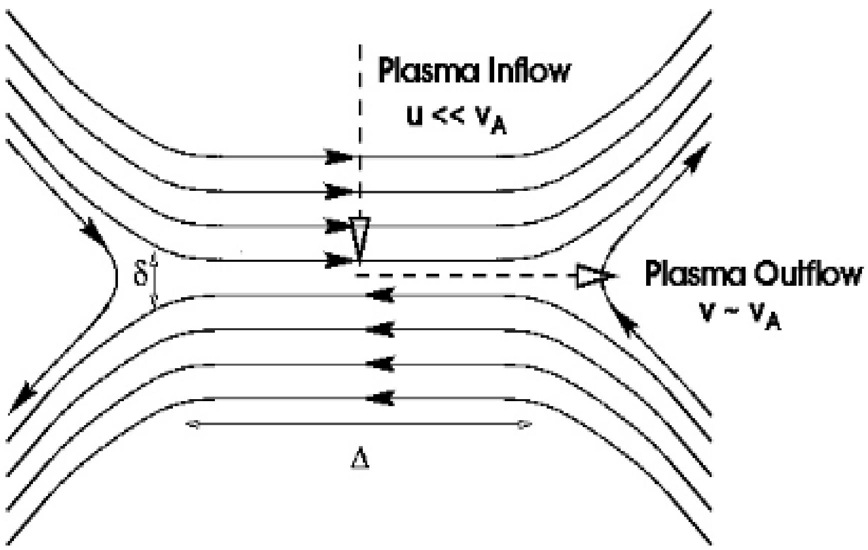

Figure 4.1: Schematic diagram of reconnection of magnetic field lines showing plasma inflow and outflow. (Image courtsey: `mrx.pppl.gov`).

Magnetic reconnection is an efficient mechanism to accelerate plasma particles to high energy in a relatively smaller time. Depending on conditions of reconnection layer several models have been proposed of conditions of thin reconnection layer. Sweet-Parker model describes a resistive diffusion of plasma materials building up high density which must escape at a speed comparable to Alfven speed v_a. This scenario corresponds to slow

reconnection rate and is not applicable to astrophysical reconnection. H.Petschek(1964) modeled fast reconnetion scenario through MHD shock and X-point geometry, but having a comparatively weaker effect. Inflow and outflow of material there is separated by slow mode shock. Reconnection rate in this model is inversely proportional to natural logarithm of Spitzer resisitivity.
However in context of plasmoid formation reconnection layer should have specific environment conditions. Highly elongated current sheets are unstable to plasmoid instability above a critical Lundquist number $S_c \sim 10^4$.

4.2 Plasmoid size distribution

4.2.1 Derivation of the plasmoid size distribution

For a compact analytical form of the plasmoid size distribution we assume a very general partial differential equation of the following form,

$$\frac{dn}{dt} = \tilde{Q} + \tilde{L}, \tag{4.1}$$

where, the $\tilde{Q}$ and $\tilde{L}$ represent the source and sink term. Now, the above expression can be rewritten in the following form,

$$\frac{dn}{dt} = v\partial_x n + \frac{dw}{dt}\partial_x n, \tag{4.2}$$

where, $\partial_t n = 0$ for steady state assumption, and v $= \frac{dx}{dt}$ is the velocity of plasmoid. The velocity can be written as , $v(w, x; x_0) = \frac{p(w,x;x_0)}{\sqrt{1+p(w,x;x_0)^2}}$, where$x_0$ is plasmoid birth location and $p \equiv \gamma\beta$, is the dimensionless four-momentum. We can again rewrite the equation in the following form,

$$\frac{dn}{dt} = v(\partial_x n + \frac{\beta_g}{pf_{sup}}\partial_w n), \tag{4.3}$$

where, $\frac{dw}{dx} = \frac{\beta_g}{pf_{sup}}$, β_g is the growth rate of plasmoid measured in a instantaneously comovimg frame of the plasmoid and f_{sup} is the growth suppresion fator. The production of te plasmoid can be written as,

$$\tilde{Q} = q_0\delta(w - w_*)S(x; 0, L), \tag{4.4}$$

where,q_0 is normalization constant and $S(y; y_1, y_2)$ is unit box function. The source term describes a generation of plasmoids of uniform size w_*. The sink term comprises of two different parts,$\tilde{L}_{adv}$ due to advection from the layer and $\tilde{L}_m$ due to merger of the plasmoids. The advection term is defined in the following way, $\tilde{L}_{adv} = -n/t_{adv}$, where the t_{adv} is defined as the time a plasmoid takes to escape the layer with local velocity,

$$t_{adv} = \epsilon \int_x^L \frac{dy}{v(w, y; x_0)}, \epsilon \geq 1. \tag{4.5}$$

Putting all these terms together we obtain,

$$\partial_x n + \frac{\beta_g \partial_w n}{pf_{sup}} = \frac{q_0\delta(w - w_*)S(x; 0, L)}{v} - \frac{n}{vt_{adv}} + L_m. \tag{4.6}$$

Now for the case of accelerating plasmoids in the limit $p \approx \frac{\beta_a(x-x_0)}{w}$. The characteristics equation then becomes, $dw/dx = \beta_g w/[\beta_a(x-x_0)]$ which has a solution of the form, $\frac{w}{w\prime} = \left(\frac{|x-x_0|}{|x\prime-x_0|}\right)^s$, where $s = \beta_g/\beta_a$. Now the equation becomes,

$$n(x, w; x_0) = \frac{q_0}{s} \int_{w_1}^{w_2} \frac{dw\prime(x\prime - x_0)\delta(w\prime - w_*)}{w\prime v(x\prime, w\prime; x_0)}, \tag{4.7}$$

where, the integration limits have been modified accordingly. The integral eventually gives,

$$n(x, w; x_0) = \frac{q_0}{c\beta_g} \sqrt{1 + \left(\frac{\beta_a(x-x_0)}{w_*}\left(\frac{w_*}{w}\right)^{\frac{1}{s}}\right)}. \tag{4.8}$$

Integration with respect to x results in,

$$n(w; x_0) = \frac{q_0}{c\beta_g} \left[\frac{x + \beta_a^2(x-x_0)^3}{6w_*^2}\left(\frac{w_*}{w}\right)^{\frac{2}{s}}\right]_{x_1}^{x_2}, \tag{4.9}$$

where, $x_1 = x_0 + x_0(w/w_*)^{1/s}$, and $x_2 = min(L, x_0 + w/w^{max}_{p\to\sqrt{\sigma}})$ and $w^{max}_{p\to\sqrt{\sigma}} = \beta_a L/\sqrt{\sigma}$. This obtains the typical size of plasmoids that can escape the layer on being significantly accelerated. Now the integration can be solved to give ultimately(with proper approximations in position),

$$N(w) \approx \frac{q_0 L}{2\beta_g c}\left(\frac{w}{w_*}\right)^{-1/s}. \tag{4.10}$$

Hence the differential position and momentum-dependent size distribution of plasmoid is a power-law with a slope $-\beta_a/\beta_g$.

4.2.2 Plasmoid distribution for simple case

Finding plasmoids in a complex system like this is difficult. As a step toward plasmoid detection we first present here our algorithm and result of detection in a very simple environment. *Nathanail et al ,2020* has presented a technique of detecting plasmoids. First they apply Gaussian smooting to image(σ image is apparently best for pronounced feature at locations of plasmoids) to remove unnecessary details (noise). Subtraction of smoothed image from original one and repeating same procedure multiple time('Difference of Gaussian') highlights the edges very sharply. Then applying Canny Edge detector algorithm on Bernoulli constant distribution detects the edge successfully. A measure of hu_t dictates whether the plasmoid is unbounded. After identifying the brightest point in the closed loop as center they found out approximate radius and size of plasmoids. They also detect large size plasmoids in this process which can potentially cause possible flaring activity in AGNs.
Magnetic reconnection is likely to take place where magnetization is high.While accreting magnetic flux small scale loops are displaced to the polar region of BH where mass density is relatively low and magnetisation is high and they reconnect there. The consequent release of magnetic energy in these plasma regions and the formation of plasmoid are then responsible for the intense variability in the emitted power. The episodic reconnection

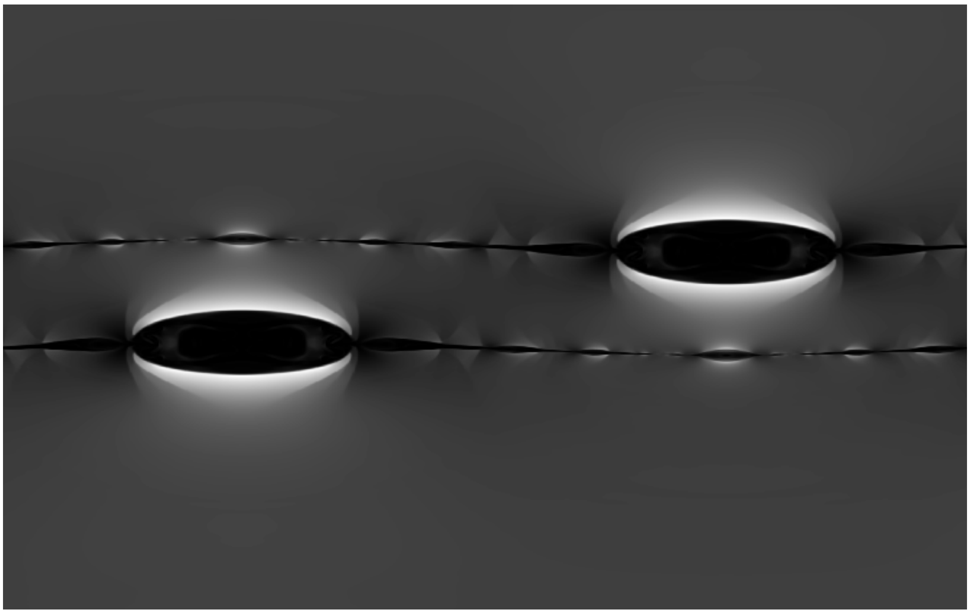

Figure 4.2: Simplistic environment with chain of plasmoids to test our algorithm. Figure shows the distribution of σ with darker at high values and lighter in low values.

that occurs close to BH can also be a source of short timescale variability.
Here we adopt an algorithm depending on general morphology of plasmoids. The simplistic environment of chain of plasmoids is shown below.

Chains of plasmoids are connected by filamentary structures which forms the 'X-point' at connection region. If observed closely bigger plasmoids actully have less magnetization at their centers and variation of σ creates artefacts inside these bubbles. While considering energetics all these details should be ignored.
Our simplistic environment with chains of plasmoids is actually a snapshot (`.vtk` files) at one particular time from a simulation of toy-model of introducing shearing effect in velocity across a current sheet that eventually reconnect magnetically to form plasmoids.

Our approach to detect these plasmoids depend on their morphological analysis.

- **Thresholding:**
  We first find a suitable threshold value to to convert the greyscale image into a binary field using python package `skimage`. The process of thresholding can also be done using the histogram of greyscale image using Otsu method. Otsu Binarization method determines a global value of threshold from the greyscale image from the image histogram. Otsu's method finds the threshold value, t such that it minimizes the weighted within-class variance for both the classes of an bimodal (having two peaks in the image histogram) or unimodal image. For our case the threshold value is 0.2 times maximum pixel value. The process of thresholding can also be done using other methods available in the `skimage` package e.g. Li method, method of local minimum etc.

- **Binary opening:**
  Binary opening on a binary field is successive operation of Binary Erosion and Minkowski Dilation on the field. Both of these are standard operations in mathematical morphology. Binary erosion or Minkowski subtraction by a structuring element produces another binary image with pixel value one at all locations (x,y) of the structuring element's origin at which the structuring element fits the morphological elements of the input image. Mathematically, Minkowski subtraction is the intersection of the binary field and the structuring element. A schematic diagram of the same is shown below in figure 4.3.

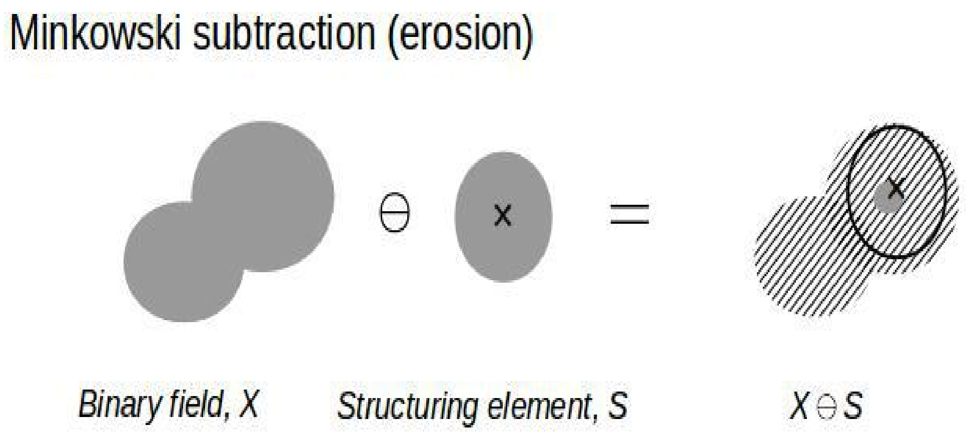

Figure 4.3: Schematic diagram of Minkowski subtraction(erosion). The grey region shows the resultant region and the shaded region indicates the original binary field in this figure.

The Minkowski addition or dilation with a structuring element, on the other hand, produces another binary image with the pixel value of one at all locations (x,y) of the origin of structuring element at which the structuring element just hits the morphological elements of the input image. Mathematically, this operation is just the union of the structuring element and the given binary field. A schematic diagram of the same is shown in figure 4.4. The successive operation of Minkowski

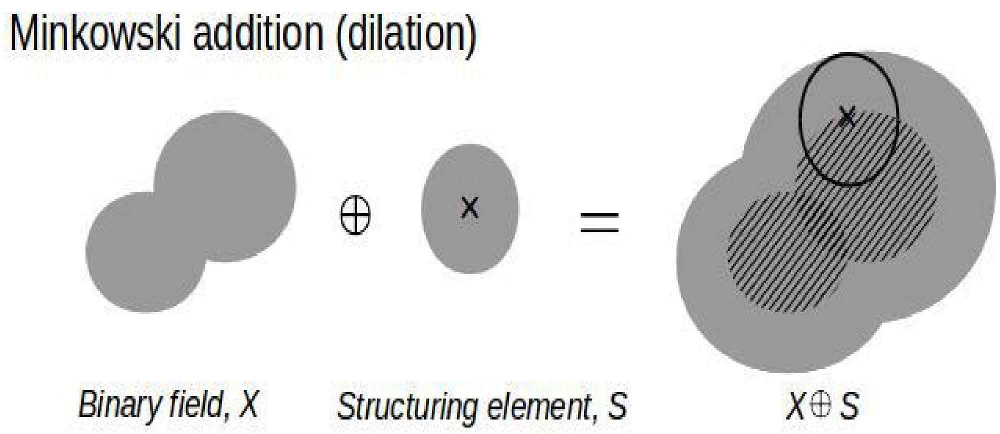

Figure 4.4: A schematic diagram of Minkowski addition or dilation. The grey area on right hand side is the resultant of the operation, whereas the shaded region shows the original input binary field.

subtraction and Minkowski addition on a given binary field is illstrsted in figure 4.5 in a step-by-step manner. Mathematically, the process of binary opening can be thought of a particular way of **sieving** of the input binary field. The intersection followed by the operation of union with same structuring element on a given binary field thus, extracts out the morphological elements that are of the almost same size of the mask.

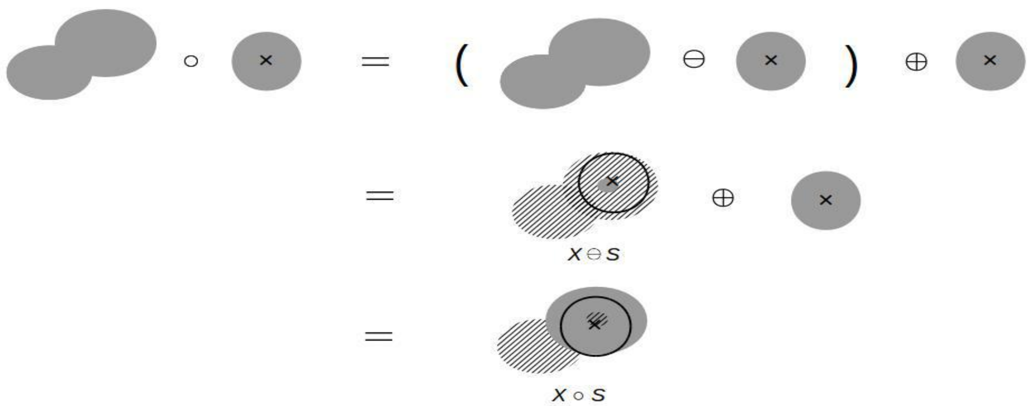

Figure 4.5: The schematic diagram of binary opening i.e. successive application of Minkowski subtraction and addition on a given binary field illustrated in step-by-step manner. Here, as before, the grey region in the final image shows the resultant region on applying the operation on the given binary field indicated in shaded region.

A mask of typical shape (circle for our case) scan the image to give only morphologies that have sizes less than the mask. We make mask of varying size scan the entire field and find structures of comparable size. The radius of mask can be taken as an equivalent radius of the plasmoids for our case as we are mainly concerned with area of the plasmoids.

The normalized number distribution is shown below in figures 4.6 and 4.7 both in regular and logarithmic scale applying the aforementioned method to the image.

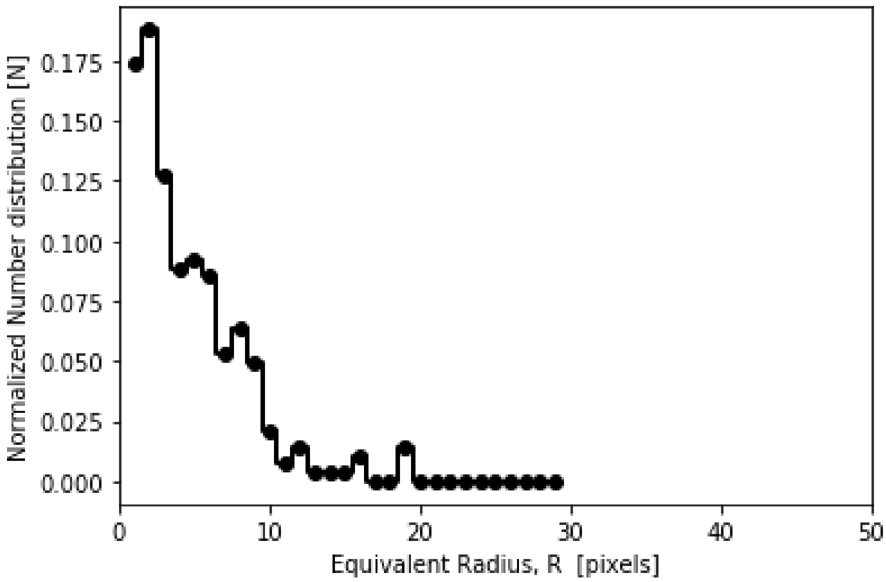

Figure 4.6: Normalized number distribution vs equivalent radius in regular scale.(This is a cumulative distribution function.)

The slope from the logarithmic plot is calculated to be **-2.06 $\pm$ 0.19** with a value of χ^2 of $\sim$ 0.002 and reduced χ^2 of 0.99, implying a decent fit which is in agreement with *Petropoulou et al, 2018*[26] where they report a power-law spectrum of number distribution of plasmoid with index consistent with our studies in a minimal extent of reconnection layer length.
The analytical expression of plasmoid size distribution in steady-state can be obtained solving a number of partial differential equation which relates the generation rate of plasmoids with superposition of a source and sink term. Petropoulou [26] have obtained an analytical expression assuming a generation of plasmoids of constant size in the process of reconnection and only loss of plasmoids is due to advection from the reconnection layers. In case of reaching upto a terminal momentum, plasmoid size distribution turns out to be a uniform one when the width of plasmoids are way lesss than the critical value dictated by the magnetization of the layer. For accelerating plasmoids the size distribution turns out to be a power-law. Physically, the overall process of formation of plasmoids through magnetic reconnection is stochastic process, involving several different processes like growth, merger, acceleration, formation at secondary current sheet (boundaries of two larger plasmoids). Hence the system is expected to have a size distribution which is power-law. The size distribution of plasmoids has been observationally found to follow a single power-law in recent studies by *R. Patel et al.*([23])regarding statistics of plasmoids associated with post-CME current sheet in solar corona. This was the first ever confirmatory evidence of models representing plasmoid size distribution to be a single power-law.

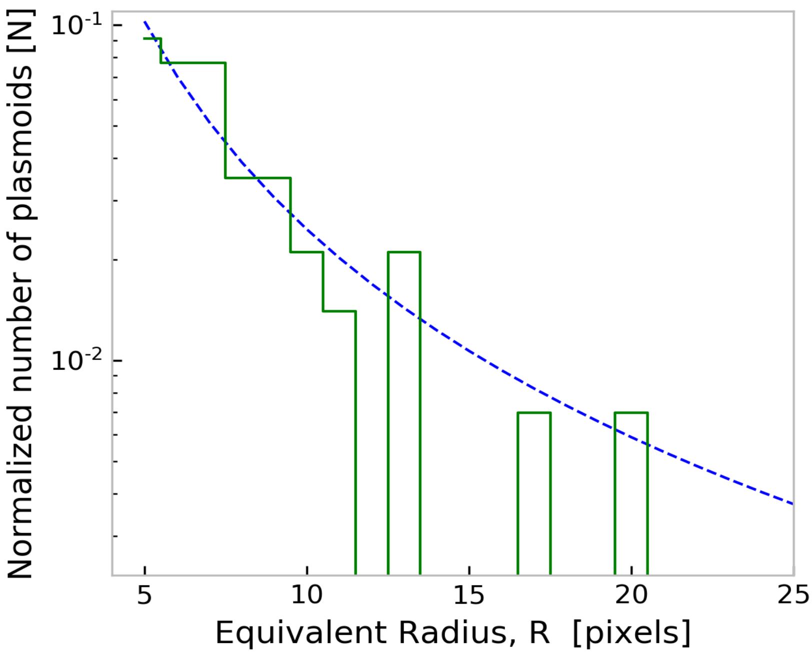

Figure 4.7: Normalized number distribution vs equivalent radius histogram (green, with y-axis in logarithmic scale) for the simple environment described in text along with the fitted power-law (blue).

To illustrate the idea that smaller size plasmoids abound in typical system and larger size plasmoid are rare we plot for our simple scenario radius× number vs radius(area × number would not be a good proxy for our case for most area is occupied by the large size bubbles in image.)

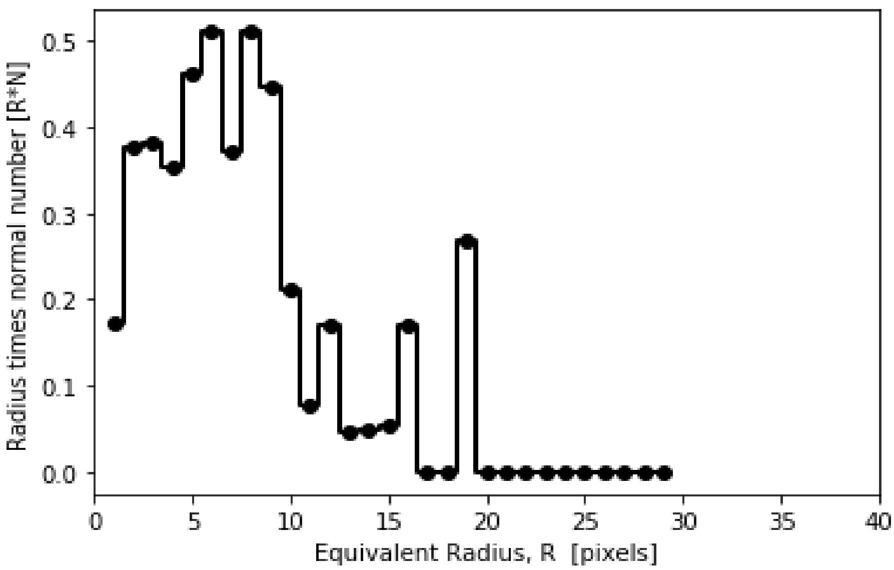

Figure 4.8: Normalized number × radius vs radius show peak indicating the radius of most abundant plasmoids.

As clearly visible from the simple image here number of plasmoids is quite low to arrive at

some statistically significant result. Yet for the plasmoids we have distribution statistics is promising and in good agreement with previous studies.
The most probable size of resulting plasmoids is small because of presence of shear in the coupled current sheet system. Due to velocity shear, which is quite common in astophysical situation, the monster plasmoids get fragmented to numerous smaller ones. So, the number of smaller plasmoids increase in the system.
A simple and straightforward calculation using causality constraint to associate variability timescale to typical lengthscale can be done assuming a characteristic lengthscale of emitting region.

$$t_{variability} = \frac{most\,probable\,radius(px) \times \frac{l_0}{total\,pixels\,of\,image}}{speed\,of\,light}. \tag{4.11}$$

If plasmoids are formed in a reconnection layer of length l_0 then our 1920 $\times$1280 pixelated simplistic image with a most probable radius of 5 pixels predict a variability timescale of $\simeq$ 43 min (which is sub-hour intra-night timescale variability) with an assumption of suitable Lorentz factor γ of 10 and size of plasmoid launching site (essentially reconnection layer length, l_0) of 0.1 pc.

Chapter 5

Validation of Detection technique

5.1 Effects of velocity shear on double current sheet system (A toy model)

Multiple current sheets with some parallel shear are quite prevalent in most astrophysical environments like pulsar magnetospheres, AGNs, heliospheric plasma etc. The explosive phase of magnetic reconnection that forms plasmoids is affected by the existence of velocity shear on the coupled current sheet. Within the framework of 2D resistive MHD, the modulation of plasmoid size distribution is investigated on a basic double current sheet system (magnetohydrodynamic).
The phenomena of acceleration of charged particles to suprathermal energies is another signature of release of copious amount of energy in magnetic reconnection process. This highly energetic particles, both ions and electrons have been observed to be present in solar flares, AGN flares and AGN jets. To validate our technique of detecting and obtaining size distribution of the plasmoids , we take up a simple setup of double current sheets with high Lundquist number in double-tearing mode with parallel velocity shear flow present across the current layers. For different values of sub-Alfvénic shear present across the layers we find out the power-law index of the size distribution of plasmoids and observe its variation with increasing shear values.

5.1.1 Numerical Setup

In the simple numerical setup, two parallel current sheets along x-axis are taken at certain separation along y-axis, in between which there is bulk flow of fluid with opposite velocity with respect to the velocities of both current sheets. Hence, there naturally is a velocity shear between the sheets. The evolution of the system is goverened by the standard resistive MHD equations in a 2D slab geometry using `PLUTO` code [18]. The computational domain is confined to a 2D region bounded by -64 to +64 in x-direction and -96 to +96 in y direction , where the numbers are in code units. The computational domain is resolved by 1280 and 1920 grid cells along x and y direction respectively. The system is considered to be isothermal and the initial magnetic field configuration is that of a double Harris-sheet equilibrium with current sheets along y = ± 16. The variation of density is set to follow the given profile:

$$\rho_y = \rho_\infty \left[\mathrm{sech}^2\left(\frac{y-16.0}{w_B}\right) + \mathrm{sech}^2\left(\frac{y+16.0}{w_B}\right) + 1.0 \right] \tag{5.1}$$

The asymptotic ρ_∞ has a value of unity here. The magnetic field profile asymptotes to a value of $\sqrt{2}$ and magnetic field shear width (w_B) is set to unity. The explicit value of resistivity (η) is taken to be 2×10^{-5} with a corresponding Lundquist number of 9×10^6. All the relevant timescales are normalised to Alfv́en transit time across the current sheets, $\tau_A = w_B/v_A$.

5.1.2 Particle Setup

Particles were introduced to the system to examine the effect of shear flow in particle acceleration. A total of 4 million particles is injected to the subset of the numerical domain which is bounded by $-64 \leq x \geq 64$ and $-40 \leq y \geq 40$. The third dimension with $-10 \leq z \geq 10$ was introduced to the domain to allow the three degrees of freedom of particles. The particles taken here have a charge to mass ratio of unity in code units corresponding to protons. With introduction of particles all length scales are normalised to the quantity, $c/\omega_{pi} = 1$, where c is the speed of light and ω_{pi} is the ion plasma frequency. The time scales are expressed in the unit of inverse cyclotron frequency, $\Omega^{-1} = c/(\omega_{pi} \times v_A)$. An extended description is given in *Paul & Vaidya, 2021* [24].

5.2 Results

The results of the study, both dynamics and distribution statistics, are listed below in two subsections.

5.2.1 Dynamical result

The systems irrespective of the values of shear show a similar evolution pattern comprising three distinct phases. The phases are, (a) a slow initial growth phase, (b) a violent explosive reconnection dominated phase, (c) a turbulent gradual relaxation phase. However, the phases are delayed in time with increasing shear velocity.
The general evolution characteristics have been described below benchmarking the zero shear velocity. In the first phase, the two monster islands form and grow gradually. The portion of current sheets outside the plasmoids start to thin gradually and fragment into smaller plasmoids. Eventually, the system enters into plasmoid-dominated explosive reconnection phase. This happens because the system tends to approach a steady-state Sweet-Parker inverse aspect ratio $\delta_{SP}/L = S^{-0.5}$. The smaller plasmoids merge into the large monster plasmoid increasing the size even larger (as can be seen from figure 1B and 2B of 5.1) and thereby enhancing the coupling between the two current sheets. It mimics the coupled double tearing mode very closely studied in *Janvier et al. (2011)* [15].

5.2.2 Reconnection rate

The reconnection rate is also explored with this study by measuring the combined reconnection rate of the two current sheets for each system following the method in *Paul & Vaidya , 2021* ([24]). The recnnection rate is found to have a tight relation with the out-of-plane electric field (E_z). The sum of the averages of the out-of-plane electric field along the two thin strips containing the current sheets gives the average reconnection

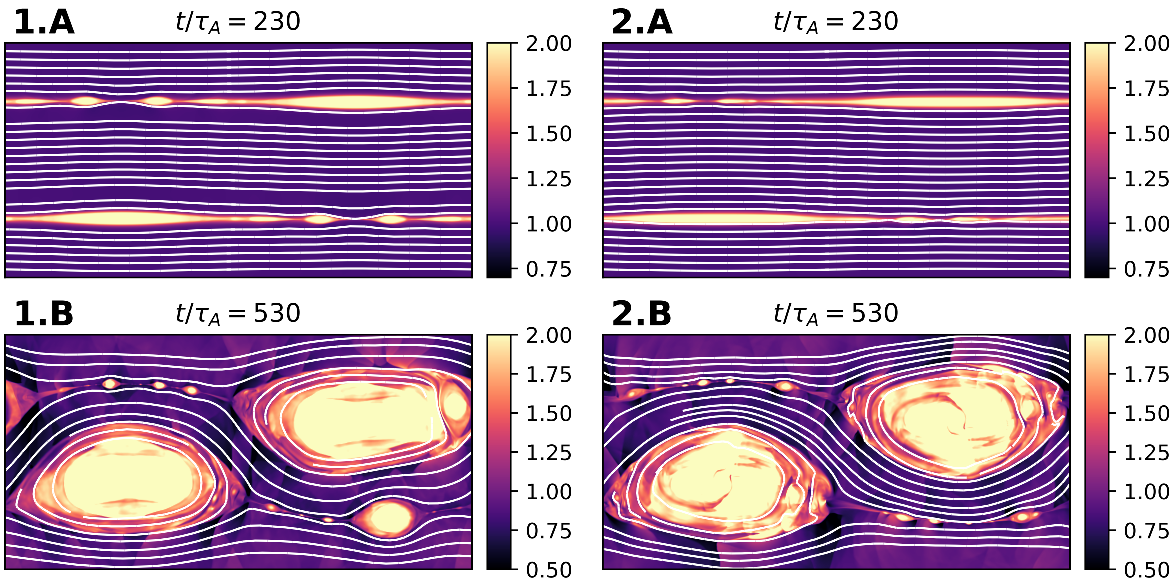

Figure 5.1: Figure shows the mass density of plasma in code units with the magnetic field streamlines overplotted. Figure numbers 1 and 2 (columns correspond to a shear speed of 0.0 v_A and 0.50 v_A respectively and the labels A and B (rows correspond to different times (t/$\tau_A \simeq$ 230 and t/$\tau_A \simeq$ 530) *Paul & Vaidya, 2021*[24]

rate. The following relation is employed to measure the same,

$$E_{\rm rec} = \frac{1}{B_0 v_{\rm A}} \left(\left\langle \left| \frac{\iint_{y_1}^{y_2} E_z dxdy}{\iint_{y_1}^{y_2} dxdy} \right| \right\rangle + \left\langle \left| \frac{\iint_{-y_1}^{-y_2} E_z dxdy}{\iint_{-y_1}^{-y_2} dxdy} \right| \right\rangle \right) \tag{5.2}$$

The relation of the velocity shear and reconnection rate is expected to have the relation , $E_{rec} = E_0 \left(1 - \frac{v_s^2}{v_A^2}\right)$, following *Cassak and Otto, 2011 ([7])*. Here, E_0 is the reconnection rate with no shear between the current sheets and the v_s is the strength of the shear flow and v_A is the local Alfvén velocity. The theoretical scaling predicts a steady decrease of reconnection rate with increase in the value of shear flow. The system is found to follow the relation quite well in the early phase of evolution when slow growth takes place. However, in the plasmoid dominated explosive reconnection phase, in high shear flow the system deviates from the relation significantly. This is mainly because of the fact that in a double current sheet system one monster plasmoid has a feedback effect on the other by pushing the magnetic flux towards the X-points of other current sheets ([15]). The larger sized magnetic islands , with lower shear speed have a significantly enhanced reconnection rate. For our case of resistive plasma, the magnetic diffusion region for fast reconnection phase is very localized. Due to formation of the large magnetic islands in an antisymmetric manner, they tend to push the magnetic flux in the direction of reconnecting X-points located above them. For lower shear speed, the magnetic islands tend to grow wide in y-direction. In this situation again the magnetic flux is displaced more toward the X-points and a strong coupling is formed between the two current sheets. This effectively increases the reconnection rate for lower shear speed in the system. For higher shear speed the flow tends to flatten the magnetic islands in the system reducing magnetic flux accumulation in direction of the X-points of the other current sheet. Hence the coupling between the double current sheet is weakened and the reconnection rate

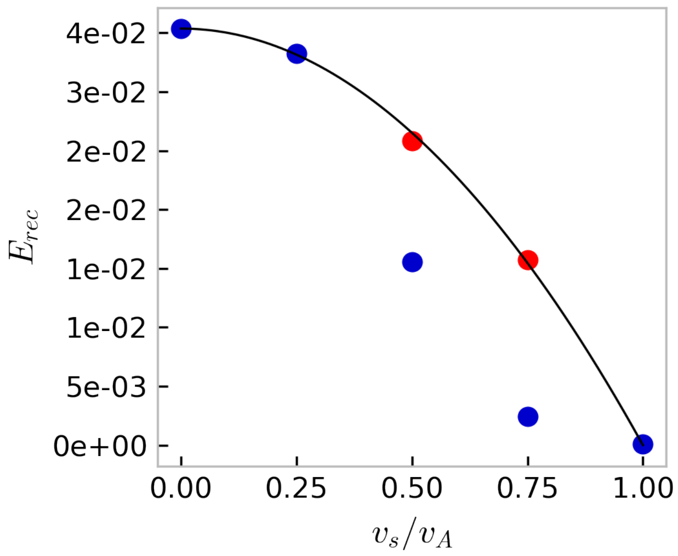

Figure 5.2: Figure shows the theoretical scaling relation by the black line. The blue circles are the reconnection rates measured during the time interval $t/\tau_A = 283$ to $t/\tau_A = 293$ for all the systems and the red circles are the reconnection rate measured at different times for the two cases as described in the text, when the magnetic islands in all the systems have same widths. *Paul & Vaidya, 2021* [24].

is reduced. However, a deviation from the theoretical scaling relation, given above, is observed in this case. It is accounted for by the unequal widths of the primary magnetic islands. For comparison the systems with shear (v_s/v_A) 0.50 and 0.75 are observed at different times ($t/\tau_A = 311$ and $t/\tau_A = 336$), when the mgnetic islands have the same width as in the case of benchmark model of zero shear speed. The red circles in figure 5.2 corresponds to the reconnection rate measured at the times mentioned above and it is evident for similar sizes of magnetic islands in the system the reconnection rate does indeed follow the theoretical scaling relation even for double tearing mode instability (DTM). It is also confirmed that the widths of the plasma magnetic islands have a feedback on the other current sheet in the system by forcing magnetic flux toward the reconnecting X-points. Even when this effect is taken into account, the reconnection rate, measured at times when the sizes of the magnetic islands are similar, is found to follow the scaling (given for the reconnection rate with shear in single current sheet) for the non-linear phases of DTM.

5.2.3 Plasmoid Size Distribution

The size distributions of plasmoids formed here at different stages of evolution are expected to be a power-law with negative indices as discussed in earlier chapters. We assume the power-law to be of the form $N(w) \sim w^{\psi}$, where ψ is a negative number between -2 and -1, within the standard uncertainty range. Here again we employ our method of granulometry recursively on the systems to obtain the size distribution of the plasmoids formed. We set an upper cutoff for the size (radius) of structural unit (circle) to be 25 pixels. On obtaining the distribution of number of plasmoids against the size of them (in pixel), the data is fitted with a power-law of the given form to observe the variation of

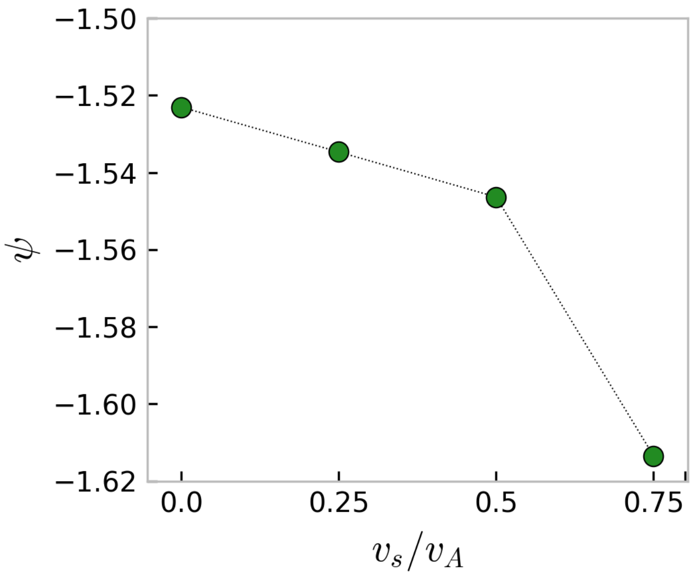

Figure 5.3: Figure shows the decreasing trend of the fitted power-law index obtained from plasmoid size distribution with increasing shear speed.

the power-law index ψ.
As mentioned above, an increase in values of shear speed flattens the widths of the primary magnetic islands weakening the reconnection rate in the non-linear explosive phase of DTM. However, the flattening of the islands facilitates further constrictions in the current sheets and reduction in the bulge of the larger islands, thereby forming several X-points in the later stages. This effectively leads to a significant number of plasmoids that are smaller in size in the system. Hence from the distribution statistics of the plasmoids, it is expected that there would be a sharp decrease in the values of power-law indices.
In figure 5.3 the variation of the index is shown with the sub-Alfvénic shear speed. The values plotted here are the median values of the fitted indices obtained from data-array between times $t/\tau_A = 50$ and $t/\tau_A = 400$, clipped at times where the variation of the indices is nearly stationary, for each shear value. The index value steadily decreases from -1.52 to -1.61. The downward trend is evident from the figure 5.3 indicating abundance of small sized plasmoids in the system. The size distribution supports the validity of single power-law for the plasmoids formed in magnetic reconnection in typical physical scenarios like explosively reconnecting double current sheet system.

5.2.4 Particle acceleration

The evolution of particle energy is studied in the plasmoid dominated explosive reconnection phase of DTM. The particles are injected at times of onset of this phase for the two different cases of shear values zero and 0.75. The energy of the particle is given by $\frac{1}{2}v_p^2$, where the v_p is the velocity of the particle. The particle energy spectrum attains a power-law with a time invariant index -1.24, irrespective of the shear values, as observed in our systems. Particles in the magnetic system show both in-plane and out-of-plane acceleration. The in-plane acceleration is explained through the encounter of particles with the shocks formed at the boundaries of the magnetic islands due to the movement of the smaller plsmoids and other magnetic structures toward the monster plasmoids with high velocities at the time of merger. Magnetic mirroring also contributes to the process of particle acceleration in the system where the particles are bounced off of the tapering ends of the bigger magnetic islands, gaining energy. The out-of-plane acceleration is caused by the out of plane electric field (E_z), which is composed of two different components, i.e. a convective term $\mathbf{v}\times\mathbf{B}$ and another resistive term($\eta\mathbf{J}$). As the particles were integrated in evolving fluid background, the out-of-plane energization has been exclusively captured in the simulation. The evolution of the particle energy spectrum is shown in the following figure 5.4. The presence of velocity shear on the flow has negligible effect on the prticle

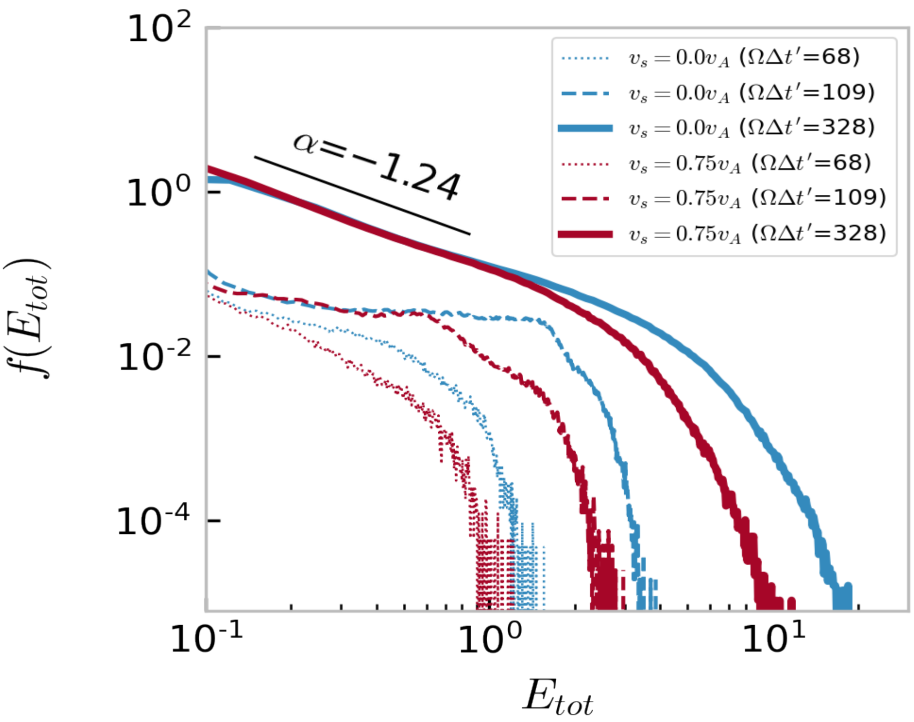

Figure 5.4: Figure shows the normalised energy spectrum of particles. The blue lines are for the case of zero shear and the red lines are for a shear magnitude of $0.75v_A$. The dotted, dashed and solid lines are representative of different integration times $\Omega\Delta t'$= 68, 109 and 328 respectively. *Paul & Vaidya, 2021* [24].

acceleration process, though in higher shear regime particle acceleration to high energy is overall less efficient. This causes the truncation of the higher energy portion of the particle energy spectrum to a smaller value as is evident from the figure 5.4 as well.

Chapter 6

Energetics of Plasmoids

6.1 Magnetic reconnection in black hole magnetosphere

Magnetic reconnection occuring in the inner magnetosphere of an accreting black hole can power a rapid and bright flares through formation of plasmoids. Accumulation of magnetic flux along with matter accretion to black hole occur simultaneously. The accumulated flux exerts an outward forceon the infalling plasma. The outward magnetic pressure on reaching a critical point, can completely stops the matter accretion, thereby producing a MAD (Magnetically Arrested Disk) like configuration (*Ramesh Narayan et al, 2003*) ([19]). Episodic eruption of the magnetic flux from the inner magnetosphere of the accreting black hole to the disk and jet funnel sheath is possible through near-event horizon reconnection. Reconnection occurs locally at the X-points where the magnetic field topology changes, as the old magnetic field line connection is destroyed and new connection takes place. At those points, the temperature of the plasma becomes very high and after that it is ejected from the layer at relativistic speed. For the flares out of some astrophysical source to account for some impulsive event of energy dissipation in short timescale, reconnetion has to be quite efficient. The reconnection is often tends to occur where the magnetization is very high. As the magnetic flux-freezing condition in the plasma in the magnetic diffusion region is not satisfied, the matters in the turbulent region get substantially rarefied. Thus the non-thermal radiation from the plasmoids passes through the tenuous, optically thin plasma formed in afore described process. In this scenario, the released magnetic energy is utilised through primarily three channels, (a) the ohmic heat energy(ηJ^2), (b) the kinetic energy of the plasmoid and (c) the non-thermal energy of particles. However, the exact partitioning of the total magnetic energy in the conversion process and physical processes for non-thermal particle acceleration are still not clearly known. We here assume, at times when the mass accretion has attained a steady rate, the magnetic reconnection produces chains of plasmoids self-sustainably. Through this process of ejecting magnetic flux tubes from the black hole magnetosphere, the accumulated magnetic flux is released to the outer region and a overall magnetic relaxation of the system is achieved. In the figure 6.1 showing the magnetic energy density, it is clearly evident that the magnetic flux accumulated in the horizon corresponds to a reservoir of magnetic energy to be channeled out via different mechanisms of magnetic flux eruptions. At the positions of X-points of the plasmoids, the plasma particles are impulsively accelerated by the effects of non-ideal electric field *(Sironi & Spitkovsky, 2014)*

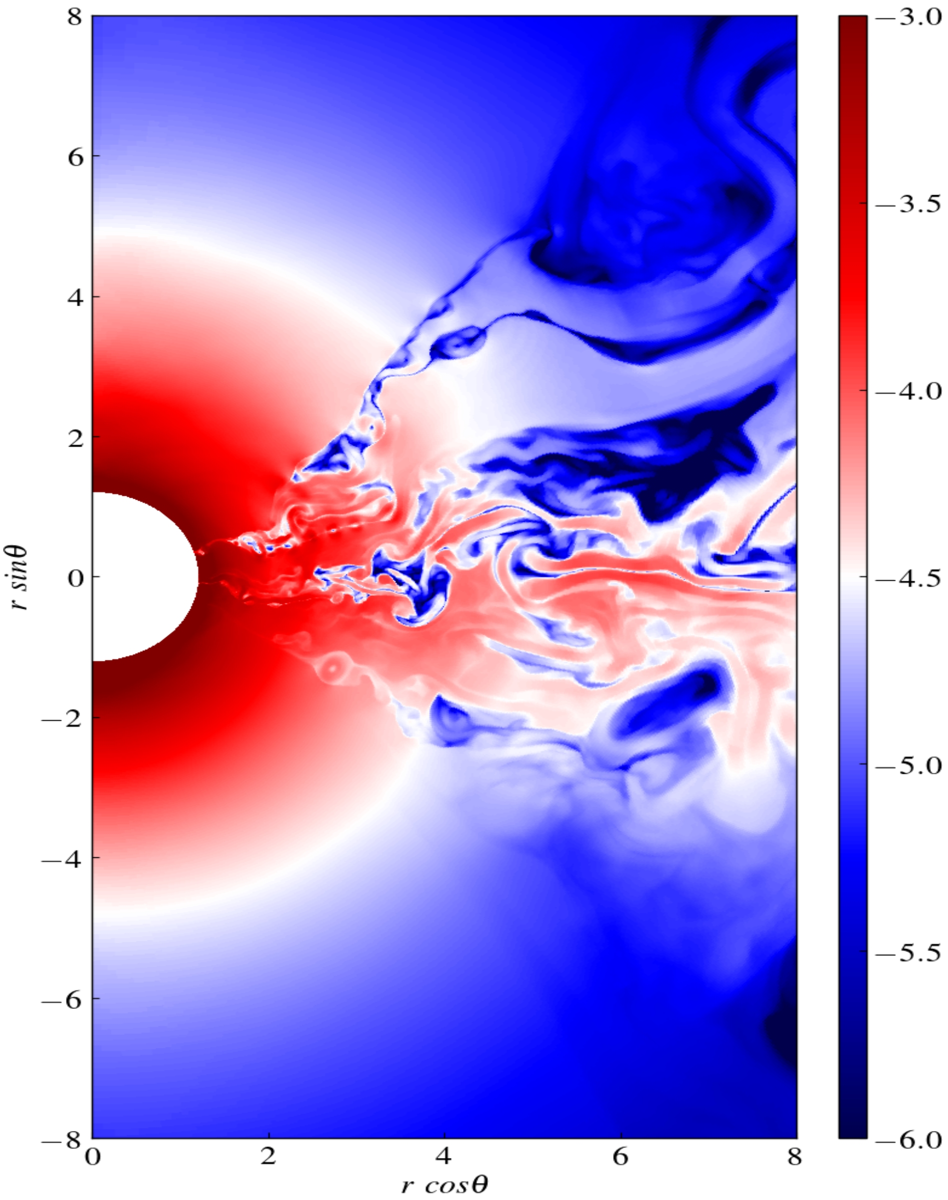

Figure 6.1: Figure shows the magnetic energy density of the disk at a time t=2000$\frac{GM}{c^3}$, indicating enhanced magnetic energy near the horizon due to flux accumulation and near-event horizon magnetic reconnection activities producing magnetic structures and plasmoids.

[37]. When these particles encounter plasmoids they undergo severe synchrotron losses. At critical accumulation rate of magnetic flux, when the mass acceretion rate is halted, a magnetosphere with equatorial current sheet can be formed. Magnetic reconnection pinches off the horizontal magnetic field there and transforms it to a vertical magnetic field, through which jet can feed the inner magnetosphere region of the black hole with highly magnetized plasma making the region conducive to explosive flux eruption events through reconnection.

6.2 Size distribution and detection of the plasmoids

From now on, we will only discuss about the statistics and energetics of plasmoids in our initially thin moderately resistive disk GRMHD setup with resistivity $\eta = 10^{-6}$ evolved to time $t = 2000$. From the distribution of Bernoulli parameter, hu_t, it is possible to detect the gravitationally unbound structures which in principle can leave the black hole system. We assume here all the outgoing blobs of plasma except the disk wind and at extreme polar regions where, jet outflow is obvious are plasmoids because current theories only predict magnetic reconnection as the only significantly efficient phenomenon of magnetic energy dissipation to power such outflow. We isolate the regions having hu_t value $\leq$ -1 as shown in the figure 3.9. To find out the size distribution and to localize the plasmoids, we need to binarize the image with proper thresholding. As there is drastic contrast in the pixel intensities in the above mentioned image, it is relatively easy to find out the threshold value using Otsu filter available in `python` package named `skimage`. As we have this unimodal image, Otsu filter is quite useful for our case. After obtaining the thresholded binary field, the method of granulometry is employed on the image to obtain the power-law size distribution of the plasmoids. Figure 6.2 shows the size distribution in logarithmic scale. The power-law slope of -1.7 $\pm$ 0.2 with a χ^2 statistic of 0.003 and reduced χ^2 close to unity ($\sim$ 0.97), supporting a good fit of the data. Though at this

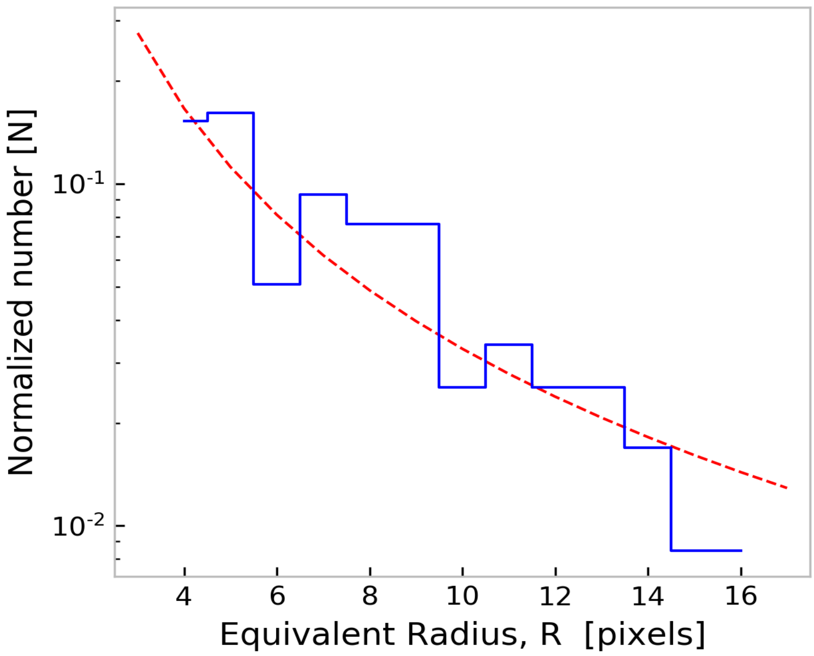

Figure 6.2: Figure shows the histogram (blue) of size (pixels) distribution of plasmoids (with y-axis in logarithmic scale) in GRMHD thin disk setup along with the fitted power-law (red).

particular time, the number of plasmoid is significantly less (21) to obtain a reliable statistics, the distribution follows the power-law very sharply. The plasmoids formed in the turbulent domain are very irregular in shape. They have very rugged contours and and apparently hard to detect with trivial 2D geometric shapes of the structuring element or the mask. However, we set the mask shape to be circular in this case too and find that the detection is totally accurate for our case. For a definite mask size (the most

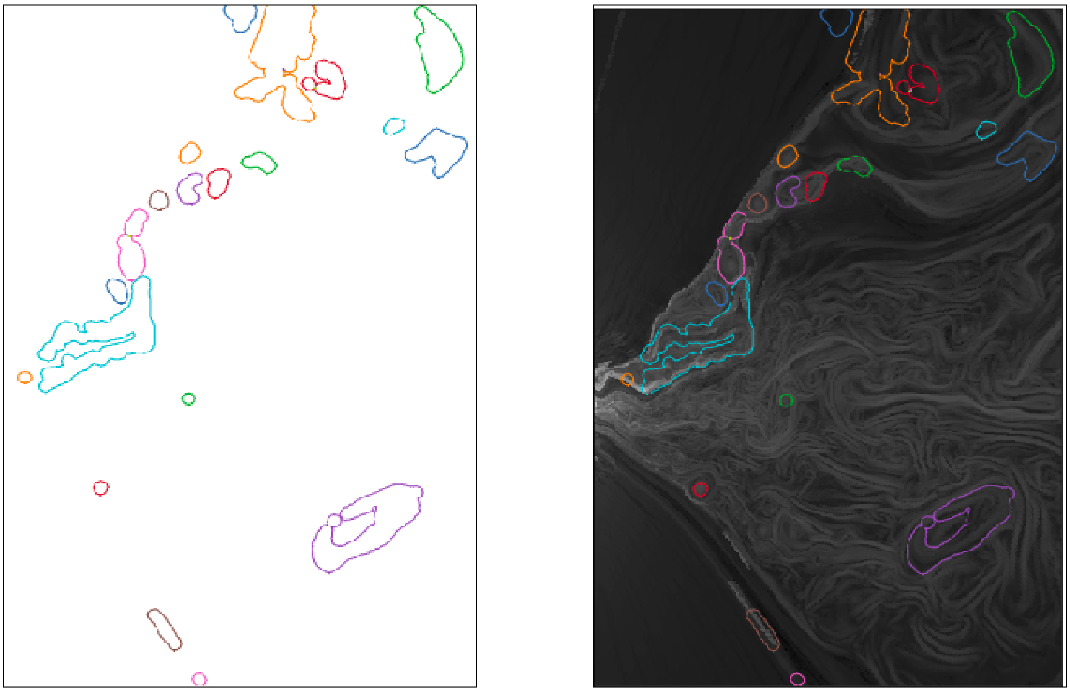

Figure 6.3: Figure on left shows the plasmoid contours as a result of applying binary opening at a stage when mask radius is 5 pixels (most probable radius) and figure on right shows the contours of detected plasmoids overplotted on the logarithmic current density plot of the same system at t = 2000.

probable radius), we distinguish the contours of the outgoing plasmoids in left figure of 6.3 and hence localize them in the field. The plasmoids with this particular size and those having larger featureless contours are detected at this stage of granlometry as is shown in left figure of 6.3. As a confirmation of the detection of plasmoids contours the current density is plotted with the contours overplotted on it in right figure of 6.3. The current sheets should coincide with contours of the plasmoid after magnetic reconnection has taken place. The exact coincidence of the current density maxima ridges with plasmoid boundary is a confirmatory test for the detection method. The magnetic field in the disk region gets thoroughly turbulent even if the simulation starts with weak seed field through the process of magnetorotational instability (MRI). Due to this turbulent magnetic field, current sheets form everywhere inside the disk. Right figure of 6.3 shows the current sheets formed in the system indicating the ubiquity of magnetic reconnection in such kind of environments.

6.3 Energy output from plasmoids

Plasmoids are constituted of highly energetic charged particles. As the magnetization is substantially high in the jet funnel sheath region, the efficiency of magnetic reconnection increases there. Inside the funnel region the magnetic field lines are sheared and twisted due to differential rotation speed of plasma at different radii. Reconnection at these sites can heats up plasma to ultra-high, relativistic temperature. This accounts for the source of energy that a portion of generated plasmoids can acquire to be gravitationally unbound. However, the plasmoids with the above conditions satisfied are not destined to escape the system, as some of them move inward to eventually fall into the black hole. The outbound plasmoids, detected from the distribution of hu_t, can actually go outside the system to cause subsequent flares. To investigate the radiation of accelerated charged particles, an approach, which is self-consistent radiative kinetic, is crucial. From the Ohmic heat energy content of the detected plasmoids, it is possible to formulate a total non-thermal emission in a consistent (although no realistic) manner. We here adopt an empirical formulation of the non-thermal emission from the plasmoids with ohmic heat content being the single source of the emission. The relativistic particles , that constitute the plasm blobs, radiate primarily through Synchrotron radiation, thereby losing its kinetic energy. In such scenario it is totally justified to assume that a certain fraction of the ohmic heat is utilised to energize this population of particles in our single-fluid plasma. Mathematically,

$$\xi \eta J^2 = m_p c^2 \int_{\gamma_{min}}^{\gamma_{max}} \gamma N_0 \gamma^{-p} d\gamma, \tag{6.1}$$

where, ξ is a fraction, m_p is the mass of proton, c is the speed of light, N_0 is the number density and γ is the particle Lorentz factor. The value of index p in plasmoid mediated magnetic reconnection regime generally has a value close to 3. Equation 6.1 has several parameters to be constrained on firm physical basis to obtain consistent energy output from the process of reconnection. As we are dealing with a 2D system, proper scaling of units is also essential for the analysis. To obtain results that are in physical units and that can directly be compared with observables from the sources, we also need to convert the relevant quantities from code units to physical units.

The ohmic heat energy content is given by the dot product of local electric field and local curent density ($E^i J_i$) at the point of interest. In left figure of 6.4, the distribution of ohmic heat energy is shown in logarithmic scale. It is important to note that even if there are several significantly hot regions, all of them do not contribute to emission due to magnetic reconnection. They may be result of excessive heating due to some other external factors like turbulent instability or viscous heating, which are not discussed here. The ohmic heating is most intense near the black hole horizon and also in the layers entering the funnel sheath region. Moreover, the component of electric field that is parallel to the current layer can effectively accelerate local particle population to super-high energy, so that the population exhibits significant deviation from a thermal energy spectrum. As we are interested in the ohmic heat energy content of the plasmoids, figure 6.4 shows the same plot of $E^i J_i$ is shown with the plasmoid boundaries over it. The total pixel intensity contained inside the contours correspond to the ohmic heat content in that region.

6.3.1 Constraining the parameters

To use the equation 6.1, we need to constrain the parameters involved in the equation. For the parameters that cannot be constrained with valid physical argument, we explore the entirety of the parameter space which is dictated by some empirical range. The parameters, ξ, γ_{min}, γ_{max} and N_0 are the parameters of interest as equation 6.1 is concerned. As the energetic particles are attched to the magnetic field lines of resulting plasmoids, the maximum relativistic gyroradius can be estimated using the average magnetic field strength in a typical plasmoid formed here. For a relativistic particle, the gyroradius is given by, $r_g = \frac{\gamma m v \perp}{|q| B}$, where the symbols have usual meanings. Now the value of γ_{max} can be constrained using the fact that the gyroradius of the particle can not be bigger than the maximal size of the plasmoid that contains it. The parameter γ_{min} can be set to a minimal practical value of 10 for such environment. The value of the fraction ξ is

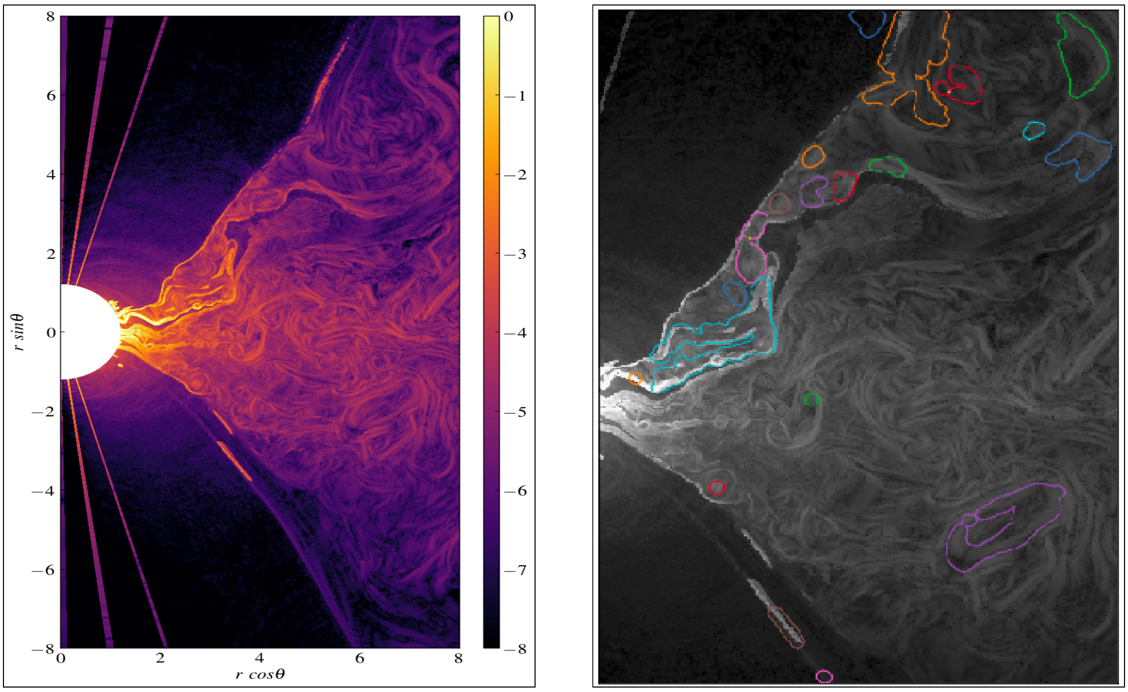

Figure 6.4: Left figure shows the ohmic heat distribution in logarithmic scale (the emanating rays are AMR artifacts). Figure on right shows the plasmoid contours overplotted on the ohmic heat energy distribution.

initially set to 0.1. With these values specified one can easily estimate the value of N_0 from equation 6.1. The number density of charged particles is one of the derived parameters that can be obtained from observatial data of such source. We here use the mass of M87* i.e. $\sim 4.8 \times 10^{42}$ gm, for conversion of the quantities to physical units. As the magnetic reconnection events occur in highly magnetized region, one usually expects a lower number density. We here estimate the number density of the plasmoids to be of the order of $10^{-4} cm^{-3}$, ranging upto a minimum of $10^{-12} cm^{-3}$. This result with fiducial values of the parameters is totally consistent with actual observational evidences. However, each of the parameters is plotted against resulting luminosity-flux for comparison in the following section.

6.3.2 Total emission energy

The particles present in the plasma undergoes severe energization by encounter with slow mode shocks and fast moving magnetic structures. The energized population then radiates via synchrotron process. For our case, the particle energy spectrum in initial state is estimated for the population of particles for each of the plasmoids. We have for a population of particles with energy spectrum, $N(E) \sim E^{-p}$, the resulting synchrotron emissivity will be $J(\nu) \sim B^{\frac{p+1}{2}} \nu^{\frac{-(p-1)}{2}}$**, upto a factor of doppler shift δ, raised to a power n whose value lies in between 2 and 3, and some constants,** where B and ν are magnetic field strength and frequency respectively. Most of the radiation is emitted in the characteristic frequency of synchrotron radiation. The characteristic frequency, which is given by $\gamma^2 \nu_g$ where, ν_g is the nonrelativistic gyrofrequency, is calculated for each plasmoid assuming uniform Lorentz factor determined by the method mentioned above.

It is important here to note that the emission integrated over the entire volume (area) of the plasmoid is astrophysical observable rather than the individual emissivities. Figure 6.5 shows the area integrated non-thermal energy output of the detected plasmoids. It is easily evident that maximum luminosity of the plasmoid can transiently attain a value of $10^{34} J/s\, or, 10^{41} erg/s$ in the rest frames of the emitting plasmoids which is consistent in observationally common flare like activities in AGNs (*Di Matteo, 1998*)([10]). It is also essential to note that the plasmoid with larger size does not necessarily output higher amount of energy as the nonthermal radiation is explicitly dependent on the number density of the charged particles in the system only. Figure 6.6 depicts the histogram of the number of plasmoids with the total energy output from them. From the figure it is inferred that most number of plasmoid emit a total radiation at a rate of $10^{34} J/s\, or, 10^{41} erg/s$ in the rest frames of the moving plasmoids.
The luminosity in the observer's frame is obtained by multiplying the emission in the plasmoid rest frame with the doppler factor δ raised to a power n. Doppler boosting effect determines the value of n to be in between 2 and 3 depending upon the geometry and spectral index of the particular source. It can be shown for a value of $n = 3$,$\gamma = 10.0$ and $\beta = \frac{v}{c} = 0.995$, and an angle close to our line of sight, the luminosity would increase 10^4 times the values observed in rest frame. For the plasmoids detected here, the emitted luminosity would increase to $10^{45} erg/s$ to the observers.

The energy output obtained here is a result of specific choice of the free parameters associated with equation 6.1. Now the parameters are varied across the entirety of their physically valid range to obtain the corresponding variation of the energy output. Figures 6.7 and 6.8 show the variation of the energy output with the variation of γ_{min} and the fraction of ohmic heat content ξ for a single particularly well-behaved plasmoid. The variation with γ_{min} shows a decreasing trend because of eliminating contribution from mildly relativistic protons with the increase in value of γ_{min}. As the value of γ_{max} is self-consistently determined from the constraint of maximal size of plasmoid, the decreasing trend is mathematically straightforward conclusion. It is interesting to note that the energy output does not change very significantly. In fact, order of magnitude change is not observed for any of the detected plasmoids in the field. It is hence inferred that **the non-thermal radiation from plasmoids formed through magnetic reconnection process has negligible dependence on the value of γ_{min}.**

For the value of ξ, the variation shows an increasing trend. As the fraction of heat produced in magnetic reconnection energizes the particles present in the reconnecting plasma, the intensity of radiation from those particles is simply increases with increasing contribution from ohmic heat content. The non-thermal energy output hence increases with as the fraction increases upto a value of unity when, in the theoretically critical limit, the total heat produced in reconnection causes non-thermal radiation from the particles by energizing and accelerating them. The value of the radiation energy **increases by two order of magnitude with increasing fraction.** From the perspective of stability, the dependence of non-thermal radiation on the fraction of ohmic heat energy content is thoroughly sensitive. This observation naturally points toward other sources of energy for the energization of the plasma particles. On the other hand, as the maximum value attained in the course of variation with the fraction is not entirely unphysical, the efficiency with which the plasma heating energizes the particle population would be worth a study. Assuming a standard luminosity of flare to be of the order of $10^{40-43} erg/s$, it is a direct conclusion that enegy is tapped from internal and kinetic energy terms. For

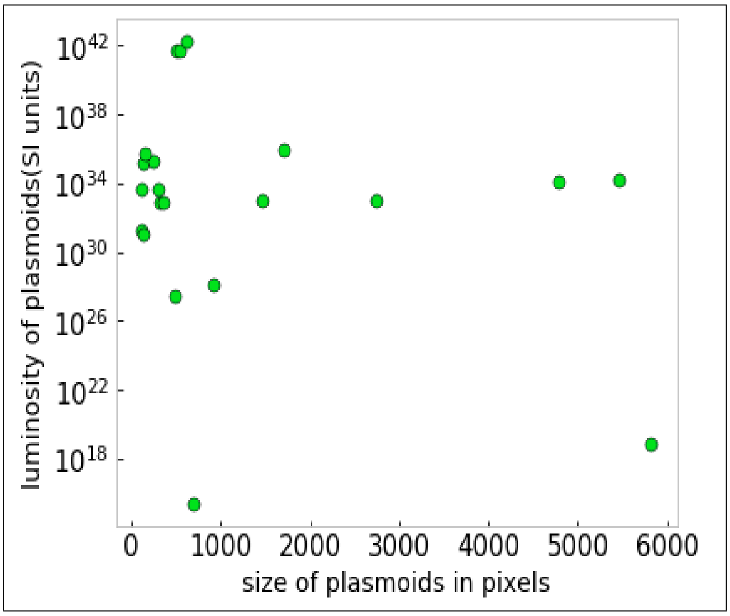

Figure 6.5: Figure shows the energy output (luminosity) of the plasmoids in the rest frames of the plasmoids against their sizes (area).

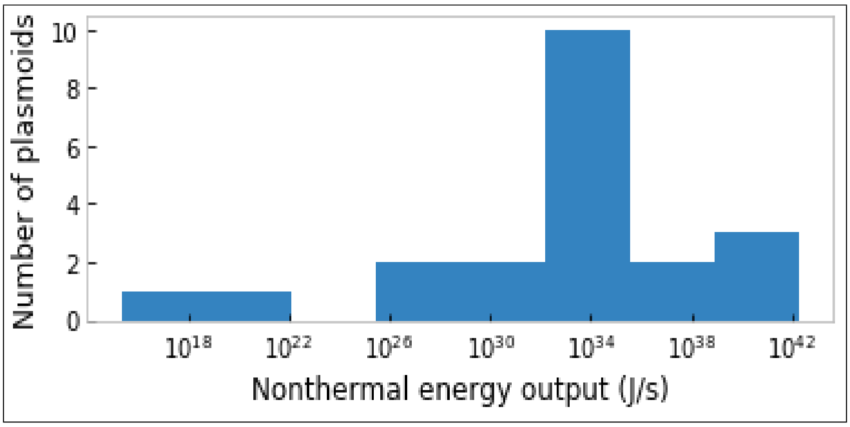

Figure 6.6: Figure shows the histogram of plasmoids number with their emitted nonthermal energies in the rest frames of the plasmoids.

this scenario under consideration shear in the bulk plasma flow can have significant effect on the particle energization as indicated in previous chapter. However, irrespective of particular reconnection dynamics and temporal evolution of plasmoids , it is here shown that, the energy output in the form of non-thermal radiation tapping energy from the ohmic heat content, can give values of flare luminosity even in higher frequency (X-ray) which is consistent with observations. The synchrotron process of energy release can liberate the kinetic energy of the particles in the plasmoids generated in turbulent magnetic reconnection process with significant efficiency. In order to explain the exact partitioning of the magnetic energy to several different forms it is necessary to thoroughly investigate the system with time by tracking a plasmoid. However, as indicated in previous studies [10], even in the presence of intense radiation field, magnetic reconnection can heat plasma to relativistic temperatures ($\times 10^9\,K$) that can cause thermal radiation even in X-ray. Here, we have also shown that inasmuch as we use the simple causality relation equation 4.11, the time scale associated with the fast variability is totally consistent with intra-night observations of flares.

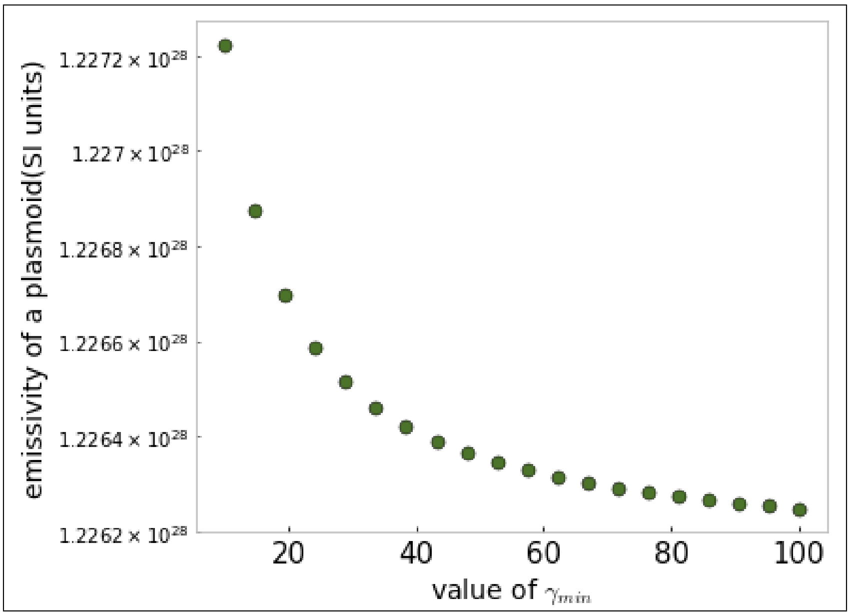

Figure 6.7: Figure shows the variation of emissivity of plasmoid with the free parameter γ_{min}.

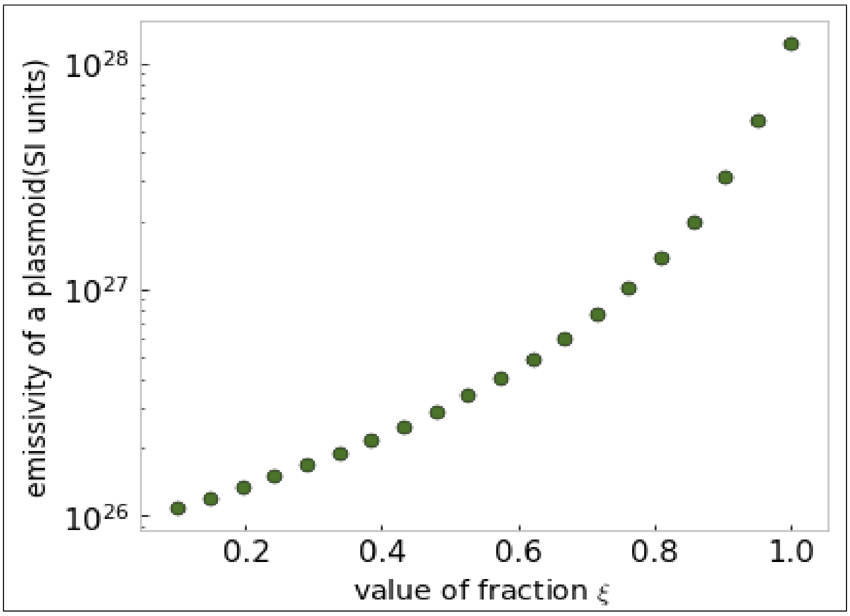

Figure 6.8: Figure shows the variation of emissivity of plasmoid with the free parameter ξ.

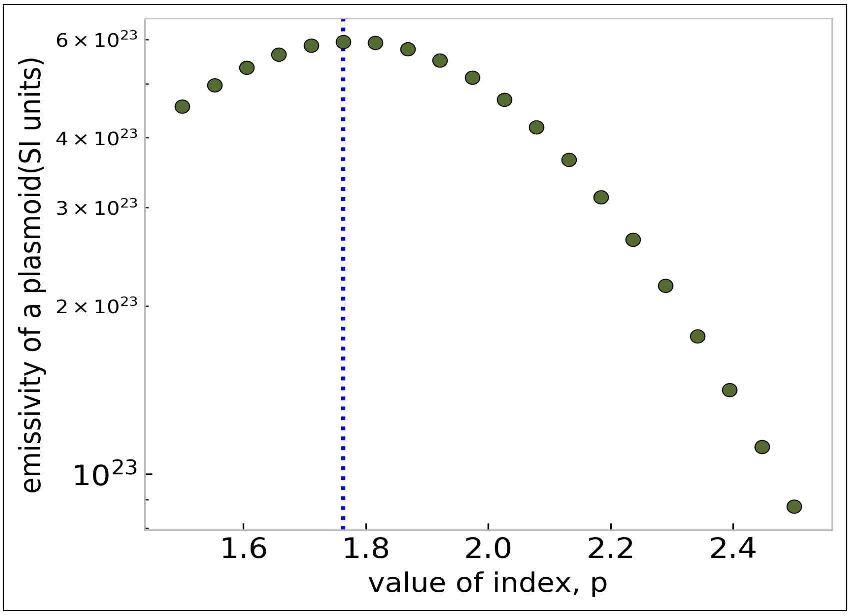

Figure 6.9: Figure shows the variation of emissivity of plasmoid with the free parameter, p.

Additionally, we investigate the dependence of the total emission on the value of energy spectrum index, p of particles. As can be seen in figure 6.9, the emissivity of the plasmoid is weakly dependent on the value of spectrum index. However, the trend is not trivial as it peaks close to a value of ~ 1.76 and then decreases steadily. This does not outright eliminates the possibility of higher value as the maximum emission does not necessarily have any serious implication on the dependent parameters supported by rigorous theoretical arguments.

Chapter 7

Summary and Outlook

7.1 Summary

- In the first part of this project we have evolved a resistive $Novikov - Thorne$ thin disk in hydrodynamic equilibrium upto a time $t = 2000$ in dimensionless unit for two different resistivity values η=10^{-10} and $\eta = 10^{-6}$. Our main result for low resistivity is formation of plasmoid through the process of magnetic reconnection mostly in off-equatorial plane where mass density is low and magnetisation has high gradient. Even in low reconnection rate due to viscosity stable plasmoids are formed in the system. For both moderately resistive disk and low resistive disk, simulation shows outflow of matter toward polar region. A lower mass density and higher magnetisation forms in simulation to effectively release plasmoids formed in reconnection. The initial magnetic field configuration is set in the only the poloidal plane with an inclination parameter. A weak perturbation in the field grows with time to eventually result in significant toroidal component in the system due to differential rotation of the matters.The turbulent nature of the magnetic field is responsible for generaating current sheets everywhere in the disk thereby facilitating reconnection. The funnel region follows a profile close to the parabolic one though it has not been explicitly fitted with given models here. While in equatorial disk region mass is being accreted funnel sheath region show matter outflow in a very efficient manner. Blandford-Payne mechanism [4] drives the disk-wind from the disk due to significant centrifugal acceleration in the locally force-free region over the equatorial plane. The Bernoulli constant distribution along with the Lorentz factor plot affirms the launching of strong Blandford-Znajek jet [3] from the material accreted in the disk. However, the disruption of the continuous disk structure is observed at time $t = 2000$ indicating turbulent magnetic flow and episodic flux eruption events from black hole magnetosphere surface.

- For a simplistic environment with prominent plasmoids in a chain we adopt binary opening to find size distribution, maximum probable size of plasmoids. Even with low plasmoid number our result is found to be in agreement with previous studies. In order to validate our detection technique, we further apply the method of granulometry to study the size distribution of plasmoids formed in an explosive plasmoid-mediated magnetic reconnection in double current sheet system where the double tearing mode instability is active. We therefore, study the effect of the sub-Alfvénic shear on resistive MHD flow. Our study finds out the modification in size distribution, the reconnection rate and the particle energy spectrum with variation of shear speed. It is inferred that the theoretical scaling relation between reconnection rate and shear speed given for a single current sheet system, hold true for double current sheet system too for identical size of primary magnetic islands. The deviation for higher shear occurs due to the feedback effect the larger islands have on the other current sheet reducing the rate of reconnection. The plasmoid size distribution forms a power-law for all the cases with different shear speeds. However, the power-law index is shown to have a decreasing trend with increasing shear magnitudes. This implies the thinning and fragmentation of the bulge of magnetic islands and the other portion of the current sheet in presence of higher shear speed. Finally, the prticle energy spectrum is observed to follow a steady power-law with index of -1.24 at a high shear value($0.75v_A$). However, the high energy tail of particle spectrum truncates at a lower value for high shea speed and smaller integration time. The physically consistent result obtained for plasmoid distribution validates the applicability of our technique of granulometry in this case too. Having obtained the most probable size of plasmoid, we show through simple calculation that a sub-hour variability timescale can be associated to the most probable lengthscale assuming a prctical and suitable pixel-to-physical length scaling relation irrespective of the nature of system under consideration.

- To explain the flaring events, bright radio flares at the center of the galaxy the energetics of the plasmoid is analysed here. We assume a simple empirical relation between the the ohmic heat energy released at the time of reconnection and the non-thermal radiation from the particles (protons) assumed to be present in the plasma of our single-fluid simulation. The radiative kinetic model has a number of free parameters. We assume some practical values for the parameters to obtain the number density of charged particles present in the system. This comes out to be consistent with the observational evidences. Next, the emission lumonosity is calculated for the plasmoids detected in the system assuming the aforementioned fiducial values. The flaring activities are successfully modeled in terms of the total energy output through the empirical relation adopted here. However, the total output is again measured for each value of the parameters for the entirety of their physically valid range to show the variation. The results obtained is physically consistent and supports the vslues we assumed at first. The radiation energy is found to have a negligible dependence on the values of γ_{min}. On the other hand, a strong dependence is observed on the fraction of ohmic heat. This naturally points toward some other sources from where energy can be tapped and the efficiency at which the released heat can energize local population of particles present in the reconnecting plasma.

7.2 Conclusions

The inner accretion region with the black hole magnetosphere region acquires large magnetization due to constant inflow from jet plasma and magnetic flux accretion. This region is therefore, prone to turbulent magnetic reconnection. On the other hand, due to turbulent nature of magnetic field in the disk current sheets are formed everywhere. Hence formation of plasmoids within a resistive accretion disk through reconnection process is very common in such scenario. These plasmoids and erupted flux tubes from black hole magnetosphere is capable of explaining the orbital motion observed after flares in the region surrounding Sgr A* by Gravity collaboration in 2018 [9]. The flaring activities observed in M87* [1] are modeled here both in terms of energrtics and the variability time-scale. We locate the plasmoids and find the size distribution of plasmoids in the accretion region which are gravitationally unbounded and can escape the system in principle to cause the subsequent energetic flaring. We employ an image processing technique called granulometry to find out the elliptical morphological structures that are the outgoing plasmoids. We show the distribution of their size follow a power-law in a number of different scenarios. However, as the plasmoids formed in reconnection gets twisted and fragmented in turbulent regions, the exact outlines of their boundaries are of secondary importance. An approximate area of the plasmoids can however, give the total heat energy content , a fraction of which, can effectively be utilised to the non-thermal radiation from the particles in the plasmoids. Alternatively, it is assumed that the non-thermal synchrotron radiation from the particles comes from the ohmic heat energy source. Even if the energy ouput turns out to be consistent, we ignore several other channels where the magnetic energy is dissipated in reconnection process. A detailed investigation of the exact partitioning of magnetic energy is important in this aspect. A study of thorough temporal evolution of the plasmoids in terms of both dynamics and energetics,though computationally expensive, is however, provide important insights into the theoretical understanding and explanation of short time scale variabilities as well as long time scale variability [10], AGN flaring activities and possibly the elusive neutrino emission from the dynamically complex energetic environment in future.

References

[1] J Albert, E Aliu, H Anderhub, LA Antonelli, P Antoranz, M Backes, C Baixeras, JA Barrio, H Bartko, D Bastieri, et al. Very high energy gamma-ray observations of strong flaring activity in m87 in 2008 february. *The Astrophysical Journal*, 685(1):L23, 2008.

[2] R. D. Blandford and D. G. Payne. Hydromagnetic flows from accretion disks and the production of radio jets. *mnras*, 199:883–903, June 1982.

[3] R. D. Blandford and R. L. Znajek. Electromagnetic extraction of energy from Kerr black holes. *mnras*, 179:433–456, May 1977.

[4] RD Blandford and DG Payne. Hydromagnetic flows from accretion discs and the production of radio jets. *Monthly Notices of the Royal Astronomical Society*, 199(4):883–903, 1982.

[5] Nikhil Borse, Sriyasriti Acharya, Bhargav Vaidya, Dipanjan Mukherjee, Gianluigi Bodo, Paola Rossi, and Andrea Mignone. Numerical study of the Kelvin-Helmholtz instability and its effect on synthetic emission from magnetized jets. *aap*, 649:A150, May 2021.

[6] Ashley Bransgrove, Bart Ripperda, and Alexander Philippov. Magnetic Hair and Reconnection in Black Hole Magnetospheres. *prl*, 127(5):055101, July 2021.

[7] PA Cassak and A Otto. Scaling of the magnetic reconnection rate with symmetric shear flow. *Physics of Plasmas*, 18(7):074501, 2011.

[8] Ritaban Chatterjee, Susmita Das, Archishman Khasnovis, Ritesh Ghosh, Neeraj Kumari, Sachindra Naik, V. M. Larionov, T. S. Grishina, E. N. Kopatskaya, E. G. Larionova, A. A. Nikiforova, D. A. Morozov, S. S. Savchenko, Yu. V. Troitskaya, I. S. Troitsky, and A. A. Vasilyev. Short-Timescale Variability of the Blazar Mrk 421 from AstroSat and Simultaneous Multi-Wavelength Observations. *arXiv e-prints*, page arXiv:2102.00919, February 2021.

[9] Gravity Collaboration et al. Spatially resolved rotation of the broad-line region of a quasar at sub-parsec scale. *Nature*, 563(7733):657–660, 2018.

[10] T Di Matteo. Magnetic reconnection: flares and coronal heating in active galactic nuclei. *Monthly Notices of the Royal Astronomical Society*, 299(1):L15–L20, 1998.

[11] Indu K. Dihingia, Bhargav Vaidya, and Christian Fendt. Jets, disc-winds, and oscillations in general relativistic, magnetically driven flows around black hole. *mnras*, 505(3):3596–3615, August 2021.

[12] G. Ghisellini, F. Tavecchio, and M. Chiaberge. Structured jets in TeV BL Lac objects and radiogalaxies. Implications for the observed properties. *aap*, 432(2):401–410, March 2005.

[13] Dimitrios Giannios, Dmitri A. Uzdensky, and Mitchell C. Begelman. Fast TeV variability in blazars: jets in a jet. *mnras*, 395(1):L29–L33, May 2009.

[14] Yi-Min Huang and A. Bhattacharjee. Distribution of Plasmoids in High-Lundquist-Number Magnetic Reconnection. *prl*, 109(26):265002, December 2012.

[15] M. Janvier, Y. Kishimoto, and J. Q. Li. Structure-Driven Nonlinear Instability as the Origin of the Explosive Reconnection Dynamics in Resistive Double Tearing Modes. *prl*, 107(19):195001, November 2011.

[16] N. F. Loureiro, R. Samtaney, A. A. Schekochihin, and D. A. Uzdensky. Magnetic reconnection and stochastic plasmoid chains in high-Lundquist-number plasmas. *Physics of Plasmas*, 19(4):042303–042303, April 2012.

[17] Eileen Meyer, Justin Finke, George Younes, Filippo D'Ammando, Bindu Rani, Sara Buson, Zorawar Wadiasingh, Ivan Agudo, Volker Beckmann, and Francesco Longo. Prospects for AGN Studies at Hard X-ray through MeV Energies. *baas*, 51(3):291, May 2019.

[18] A. Mignone, G. Bodo, S. Massaglia, T. Matsakos, O. Tesileanu, C. Zanni, and A. Ferrari. PLUTO: A Numerical Code for Computational Astrophysics. *apjs*, 170(1):228–242, May 2007.

[19] Ramesh Narayan, Igor V Igumenshchev, and Marek A Abramowicz. Magnetically arrested disk: an energetically efficient accretion flow. *Publications of the Astronomical Society of Japan*, 55(6):L69–L72, 2003.

[20] Antonios Nathanail, Christian M. Fromm, Oliver Porth, Hector Olivares, Ziri Younsi, Yosuke Mizuno, and Luciano Rezzolla. Plasmoid formation in global GRMHD simulations and AGN flares. *mnras*, 495(2):1549–1565, June 2020.

[21] I. D. Novikov and K. S. Thorne. Astrophysics of black holes. In *Black Holes (Les Astres Occlus)*, pages 343–450, January 1973.

[22] Hector Olivares, Oliver Porth, Jordy Davelaar, Elias R. Most, Christian M. Fromm, Yosuke Mizuno, Ziri Younsi, and Luciano Rezzolla. Constrained transport and adaptive mesh refinement in the Black Hole Accretion Code. *aap*, 629:A61, September 2019.

[23] Ritesh Patel, Vaibhav Pant, Kalugodu Chandrashekhar, and Dipankar Banerjee. A statistical study of plasmoids associated with a post-cme current sheet. *Astronomy & Astrophysics*, 644:A158, 2020.

[24] Arghyadeep Paul and Bhargav Vaidya. Effects of a velocity shear on double current sheet systems: Explosive reconnection and particle acceleration. *Physics of Plasmas*, 28(8):082903, August 2021.

[25] J. Peitz and S. Appl. *On viscous disc flows around rotating black holes*, volume 487, page 209. 1997.

[26] M. Petropoulou, I. M. Christie, L. Sironi, and D. Giannios. Plasmoid statistics in relativistic magnetic reconnection. *mnras*, 475(3):3797–3812, April 2018.

[27] M. Petropoulou, K. Nalewajko, M. Hayashida, and A. Mastichiadis. A hadronic minute-scale GeV flare from quasar 3C 279? *mnras*, 467(1):L16–L20, May 2017.

[28] G. Ponti, E. George, S. Scaringi, S. Zhang, C. Jin, J. Dexter, R. Terrier, M. Clavel, N. Degenaar, F. Eisenhauer, R. Genzel, S. Gillessen, A. Goldwurm, M. Habibi, D. Haggard, C. Hailey, F. Harrison, A. Merloni, K. Mori, K. Nandra, T. Ott, O. Pfuhl, P. M. Plewa, and I. Waisberg. A powerful flare from Sgr A* confirms the synchrotron nature of the X-ray emission. *mnras*, 468(2):2447–2468, June 2017.

[29] Oliver Porth, Hector Olivares, Yosuke Mizuno, Ziri Younsi, Luciano Rezzolla, Monika Moscibrodzka, Heino Falcke, and Michael Kramer. The black hole accretion code. *Computational Astrophysics and Cosmology*, 4(1):1, May 2017.

[30] S. M. Ressler, E. Quataert, and J. M. Stone. Hydrodynamic simulations of the inner accretion flow of Sagittarius A* fuelled by stellar winds. *mnras*, 478(3):3544–3563, August 2018.

[31] Luciano Rezzolla and Olindo Zanotti. *Relativistic Hydrodynamics*. 2013.

[32] H. Riffert and H. Herold. Relativistic Accretion Disk Structure Revisited. *apj*, 450:508, September 1995.

[33] Ni I Shakura and Rashid Alievich Sunyaev. Black holes in binary systems. observational appearance. *Astronomy and Astrophysics*, 24:337–355, 1973.

[34] Kazunari Shibata and Syuniti Tanuma. Plasmoid-induced-reconnection and fractal reconnection. *Earth, Planets and Space*, 53:473–482, June 2001.

[35] A. Shukla, K. Mannheim, S. R. Patel, J. Roy, V. R. Chitnis, D. Dorner, A. R. Rao, G. C. Anupama, and C. Wendel. Short-timescale γ-Ray Variability in CTA 102. *apjl*, 854(2):L26, February 2018.

[36] Lorenzo Sironi, Dimitrios Giannios, and Maria Petropoulou. Plasmoids in relativistic reconnection, from birth to adulthood: first they grow, then they go. *mnras*, 462(1):48–74, October 2016.

[37] Lorenzo Sironi and Anatoly Spitkovsky. Relativistic reconnection: an efficient source of non-thermal particles. *The Astrophysical Journal Letters*, 783(1):L21, 2014.

[38] Fabrizio Tavecchio and Gabriele Ghisellini. Structured jets and VHE emission of blazars and radiogalaxies. In Felix A. Aharonian, Werner Hofmann, and Frank Rieger, editors, *American Institute of Physics Conference Series*, volume 1085 of *American Institute of Physics Conference Series*, pages 431–434, December 2008.

[39] D. A. Uzdensky, N. F. Loureiro, and A. A. Schekochihin. Fast Magnetic Reconnection in the Plasmoid-Dominated Regime. *prl*, 105(23):235002, December 2010.

[40] Itin Yakov. M. p. hobson, g. p. efstathiou and a. n. lasenby (eds): General relativity: an introduction for physicists. *General Relativity and Gravitation*, 40:1807–1808, 08 2008.